Johann Radon Institute for
Computational and Applied Mathematics
Austrian Academy of Sciences (ÖAW)

Discontinuous Galerkin Isogeometric Analysis for parametrizations with overlapping regions

C. Hofer, I. Toulopoulos

RICAM-Report 2017-07

Discontinuous Galerkin Isogeometric Analysis for parametrizations with overlapping regions.

Christoph Hofer[1] and Ioannis Toulopoulos[2]

1 Johannes Kepler University (JKU),
Altenbergerstr. 69, A-4040 Linz, Austria,

2 Johann Radon Institute for Computational and Applied Mathematics (RICAM),
Austrian Academy of Sciences
Altenbergerstr. 69, A-4040 Linz, Austria,

christoph.hofer@jku.at
ioannis.toulopoulos@ricam.oeaw.ac.at

Abstract. The Isogeometric Analysis (IgA) of boundary value problems in complex domains often requires a decomposition of the computational domain into patches such that each of which can be parametrized by some geometrical mapping. The decomposition can include non-matching parametrizations of the interfaces, i.e., the interfaces of the adjacent patches may be not identical. The lack of the exact parametrization of the physical patches can lead to the creation of overlapping regions between the patches. In this case, the whole error includes two parts: the first part is related to the incorrect geometric representation of the patches and the second part is related to the approximation properties of the method. In this paper, we analyze the two errors separately. The study of the error related to the incorrect parametrization of the patches is treated as a non-consistent error caused by a geometric perturbation of the patches. The second error part is estimated by following classical IgA error discretization analysis. We present numerical results of a series of test problems that validate the theoretical estimates.

Key words: Elliptic diffusion problems, Heterogeneous diffusion coefficients, Isogeometric Analysis, Non-matching parametrized interfaces, overlapping patches, Discontinuous Galerkin methods, consistency error.

1 Introduction

Isogeometric Analysis (IgA) has been introduced in [21] as a new methodology for solving numerically Partial Differential Equations (PDE) considered in complicated domains. The key idea of the IgA concept is to use the superior finite dimensional spaces, which are used in Computer Aided Design (CAD), e.g., B-splines, NURBS, for both, the exact representation of the computational domain Ω and for discretizing the PDE problem. Since this work, many applications of IgA methodology to several fields have been discussed in several papers, see e.g., the monograph [7] and the references within and the survey paper [8]. From computational point of view, we can say that the numerical algorithm for constructing the the B-spline (or NURBS) basis functions is quite simple and this helps extremely in the production of high order approximate solutions. Furthermore, IgA offers a particular suitable frame for developing $h-p$ (here p is the B-spline degree) adaptivity methods with a possible change of the inter-element smoothness, [7]. From theoretical point of view, the fundamental approximation properties of the B-spline spaces on a reference domain are discussed in [34] and the approximation properties of the mapped B-spline (or NURBS) spaces, which indeed are used to discretize the PDE problem, are discussed in several papers, see e.g., [4], [35],[8], [25].

In realistic applications, it is usually more preferable the computational domain Ω to be decomposed into a union of non-overlapping patches (subdomains), i.e., $\overline{\Omega} = \cup_{i=1}^{N} \overline{\Omega_i}$. For example, when Ω is a domain with complex geometry and different PDE models are used in different parts of Ω, it is more convenient to consider each of these parts as a separate patch. Each patch Ω_i is viewed as an image of an associated parametrization mapping. These mappings are linear combinations of basis functions of the B-splines spaces. The vector valued coefficients describe the shape of the patch and are called control points. There have been presented several segmentation techniques and procedures for splitting complex domains into simpler subdomains and

defining their control nets, see, e.g., [22], [29], [20]. Usually, one obtains compatible parametrizations of the patches in the sense that the parameterizations of adjacent patches lead to identical interfaces. Then using the same patch-wise defined B-spline spaces, the discretization of the PDE model can be completed. If we consider B-spline spaces without continuity requirements across the interfaces discontinuous Galerkin (dG) techniques (or Nitsche's type treatment) can be applied for coupling the local patch-wise discrete problems, see e.g., [3], [33],[28],[25].

However, when the patches have complex topology, it is possible to get a non-conforming parametrization of the patch interfaces, this means that the patch interfaces are not identical. More precisely, during the construction of the parametrization of a patch, lets say Ω_i, the control points which are related to an interface may have not appropriately been determined with the corresponding control points of the adjacent patch Ω_j for $i \neq j$. This results in an IgA patch decomposition of Ω that can have gap and/or overlapping regions between Ω_i and Ω_j, see Fig. 1(b). We call these decompositions non-matching interface IgA parametrizations, or some times segmentation crimes. If we apply our IgA methodology for solving the PDE problem on a such decomposition, a direct consequence is that the whole discretization error will include two (main) parts: the first is coming naturally from the approximation properties of the B-spline spaces and the second part is coming due to the incorrect representation of the patch geometry. Furthermore, due to the non-matching interior patch interfaces, a direct application of the dG numerical fluxes proposed in [25] is not possible, because we can not immediately estimate the jump of the normal fluxes on the non-matching faces. In our recent papers, [17] and [19], we developed discontinuous Galerkin IgA (dG IgA) numerical schemes for solving problems on non-matching interface parametrizations including only gap regions. In particular, as a model problem, we consider a linear diffusion problem with discontinuous coefficients, lets say ρ, and we perform an IgA decomposition of Ω compatible with coefficient ρ, i.e., the restriction ρ_i of ρ to each Ω_i is constant. Then we apply Taylor expansions across the gap width d_g, using known interior patch values of the solution in order to estimate the unknown jumps of the normal fluxes on the non-matching interfaces. Finally, we used these estimates and the Taylor expansions for constructing suitable dG numerical fluxes that helped us on the weakly coupling of the local discrete problems. We showed a priory estimates in the dG-norm, expressed in terms of the mesh size and the gap width, i.e., $\mathcal{O}(h^r) + \mathcal{O}(d_g)$, where r depends on the B-spline degree p and the regularity of the solution. The gap width d_g is a quantity that measures the distance of two diametrically opposite points on the boundary of the gap region. In [17] and [19], we have shown that, if $d_g = \mathcal{O}(h^{p+\frac{1}{2}})$, the proposed dG IgA scheme has optimal approximation properties.

In [18], we apply the same approach as in [17] and [19], for solving the same PDE problem on decompositions that can also include simple overlapping regions between two different patches, lets say Ω_i and Ω_j. In [18], we did not present separate estimates for the error coming from the co-appearance of different diffusion coefficients ρ_i and ρ_j on the overlapping region $\Omega_i \cap \Omega_j$. In this work, we extend the previous concept to cases of having more general overlapping regions, and we present an error investigation in a different spirit. In particular, first we consider auxiliary, also called perturbed, variational problems, which are compatible with the overlapping IgA representation of the patches. We denote their solutions by u^*. These problems are not consistent in the sense that the original physical solution u does not satisfy them. Then, we proceed and discretize the perturbed problems. We treat the whole error, as an error caused by a domain perturbation. We decompose it into two components. The first is related to the approximation of the jumps of the solution on the non-matching interfaces. Here we follow the same ideas as in [17] and [19]. The second error component can be characterized as consistency error. It is related to the coexistence of different ρ_i and ρ_j on the overlapping region $\Omega_i \cap \Omega_j$. The different diffusion coefficients forces us to discretize two different problems on the overlaps. In other words, the numerical scheme under consideration produces two different numerical solutions on the overlapping regions associated with the two different diffusion coefficients. The produced

numerical solutions have optimal approximation properties associated with u^*, but we can not directly infer that they can approximate in an optimal way the solution u of the original physical problem. In the present paper, we first provide an estimate for the consistency error $u - u^*$ and then an estimate for the approximation error $u - u_h^*$. Under appropriate assumptions imposed on the data of the continuous problem, we show that the error $\|\nabla(u - u*)\|_{L^2}$ can be bounded in terms of the overlapping width d_o. Then, for the spacial case where d_o is of order h^λ, $\lambda \geq 1$, we show that the whole approximation error can be estimated in terms of $h^{\lambda-\frac{1}{2}}$.

We note that IgA decompositions with non-matching interfaces meshes, overlapping regions even trimmed patches have been considered in many publications. For the communication of the discrete patch-wise problems, several Nitsche's type coupling methods involving normal flux terms have been applied across the interfaces, see e.g., [33],[28],[3],[5] and the references therein. To the knowledge of the authors, there are no works that analytically discuss estimates for the error, which is caused by the incorrect representation of the shape of the patches. The purpose of this work is to present a such error analysis.

Lastly, we mention that, for the solution of PDE problems in complex domains, finite element methods on overlapping meshes have been proposed, mainly in the frame of Schwarz alternating method [30],[27], see e.g., [6],[2],[1] and the references therein. In these approaches, Nitsche's techniques have been applied on the intersection faces of the overlapping meshes for coupling the local problems. The main difficulty in these approaches is the computation of the intersections between the two overlapping meshes, which include *cut* mesh elements of arbitrary shape. This may lead to further difficulties on the construction of the finite element spaces on the intersection regions. The introduction of this methodology into IgA frame described here, is not easily applicable, because this approach would require the solution of non-linear system for finding the cut mesh points. The dG IgA approach that is presented in this work seems to be more flexible and can be easily implemented and generalized even for more realistic problems.

The structure of the paper is as follows: Section 2 presents the PDE model, briefly reviews the B-spline spaces and describes the case of having non-matching parametrized interfaces with overlapping regions. Section 3, presents in detail the perturbation problems, the bounds for the consistency error, the proposed dG IgA scheme and the error analysis. Section 4, includes several numerical examples that confirm the theoretical estimates. The paper closes with the Conclusions.

2 The model problem

2.1 Preliminaries

Let Ω be a bounded Lipschitz domain in $\mathbb{R}^d$, $d = 2, 3$, and let $\boldsymbol{\alpha} = (\alpha_1, \ldots, \alpha_d)$ be a multi-index of non-negative integers $\alpha_1, \ldots, \alpha_d$ with degree $|\boldsymbol{\alpha}| = \sum_{j=1}^d \alpha_j$. For any α, we define the differential operator $D^{\boldsymbol{\alpha}} = D_1^{\alpha_1} \ldots D_d^{\alpha_d}$, with $D_j = \partial/\partial x_j$, $j = 1, \ldots, d$, and $D^{(0,\ldots,0)}\phi = \phi$. For a non-negative integer m, let $C^m(\Omega)$ denote the space of all functions $\phi : \Omega \to \mathbb{R}$, whose partial derivatives $D^{\boldsymbol{\alpha}}\phi$ of all orders $|\boldsymbol{\alpha}| \leq m$ are continuous in Ω. Let ℓ be a non-negative integer. As usual, $L^2(\Omega)$ denotes the Sobolev space for which $\int_\Omega |\phi(x)|^2\, dx < \infty$, endowed with the norm $\|\phi\|_{L^2(\Omega)} = \big(\int_\Omega |\phi(x)|^2\, dx\big)^{\frac{1}{2}}$, and $L^\infty(\Omega)$ denotes the functions that are essentially bounded. Also

$$H^\ell(\Omega) = \{\phi \in L^2(\Omega) : D^{\boldsymbol{\alpha}}\phi \in L^2(\Omega), \text{ for all } |\alpha| \leq \ell\},$$

denote the standard Sobolev spaces endowed with the following norms

$$\|\phi\|_{H^\ell(\Omega)} = \big(\sum_{0\leq|\alpha|\leq\ell} \|D^{\boldsymbol{\alpha}}\phi\|^p_{L^2(\Omega)}\big)^{\frac{1}{2}},$$

and by $H^{\frac{1}{2}}(\partial\Omega)$ we denote the trace space of $H^1(\Omega)$. We identify L^2 and H^0 and also define the subspace $H^1_0(\Omega)$ and $H^1_\Gamma(\Omega)$ of $H^1(\Omega)$

$$H^1_0(\Omega) = \{\phi \in H^1(\Omega) : \phi = 0 \,\text{on}\, \partial\Omega\}, \quad H^1_\Gamma(\Omega) = \{\phi \in H^1(\Omega) : \phi = 0 \,\text{on}\, \Gamma \subset \partial\Omega\}.$$

We recall Hölder's and Young's inequalities

$$\left|\int_\Omega \phi_1\phi_2\, dx\right| \leq \|\phi_1\|_{L^2(\Omega)}\|\phi_2\|_{L^2(\Omega)} \quad \text{and} \quad \left|\int_\Omega \phi_1\phi_2\, dx\right| \leq \frac{\epsilon}{2}\|\phi_1\|^2_{L^2(\Omega)} + \frac{1}{2\epsilon}\|\phi_2\|^2_{L^2(\Omega)}, \tag{2.1}$$

that hold for all $\phi_1 \in L^2(\Omega)$ and $\phi_2 \in L^2(\Omega)$ and for any fixed $\epsilon \in (0, \infty)$. In addition, we recall trace and Poincare's inequalities, [13],

$$\begin{aligned} \|\phi\|_{L^2(\partial\Omega)} \leq & C_{tr}\|\phi\|^2_{L^2(\Omega)}\|\phi\|^2_{H^1(\Omega)}, \\ \|\phi\|_{L^2(\Omega)} \leq & \text{meas}_{\mathbb{R}^d}(\Omega)\, \|\nabla\phi\|^2_{L^2(\Omega)}, \quad \text{for} \quad \phi \in H^1_\Gamma(\Omega). \end{aligned} \tag{2.2}$$

2.2 The elliptic diffusion problem

We shall consider the following elliptic Dirichlet boundary value problem

$$-\text{div}(\rho\nabla u) = f \text{ in } \Omega \quad \text{and} \quad u = u_D \text{ on } \partial\Omega \tag{2.3}$$

as model problem. The weak formulation of the boundary value problem (2.3) reads as follows: for given source function $f \in L^2(\Omega)$ and Dirichlet data $u_D \in H^{1/2}(\partial\Omega)$, the trace space of $H^1(\Omega)$, find a function $u \in H^1(\Omega)$ such that $u = u_D$ on $\partial\Omega$ and the variational identity

$$a(u, \phi) = l_f(\phi),\ \forall\phi \in H^1_0(\Omega), \tag{2.4}$$

is satisfied, where the bilinear form $a(\cdot,\cdot)$ and the linear form $l_f(\cdot)$ are defined by

$$a(u, \phi) = \int_\Omega \rho\nabla u\nabla\phi\, dx \quad \text{and} \quad l_f(\phi) = \int_\Omega f\phi\, dx, \tag{2.5}$$

respectively. The given diffusion coefficient $\rho \in L^\infty(\Omega)$ is assumed to be uniformly positive and piecewise (patchwise, see below) constant. These assumptions ensure existence and uniqueness of the solution due to Lax-Milgram's lemma. For simplicity, we only consider pure Dirichlet boundary conditions on $\partial\Omega$. However, the analysis presented in our paper can easily be generalized to other constellations of boundary conditions which ensure existence and uniqueness such as Robin or mixed boundary conditions.

In what follows, positive constants c and C appearing in inequalities are generic constants which do not depend on the mesh-size h. In many cases, we will indicate on what may the constants depend for an easier understanding of the proofs. Frequently, we will write $a \sim b$ meaning that $c\, a \leq b \leq C\, a$.

2.3 Decomposition into patches

In many practical situations, the computational domain Ω has a multipatch representation, i.e., it is decomposed into N non-overlapping patches $\Omega_1, \Omega_2, \ldots, \Omega_N$, (also called subdomains):

$$\overline{\Omega} = \bigcup_{i=1}^{N} \overline{\Omega}_i, \quad \text{with } \Omega_i \cap \Omega_j = \emptyset, \text{ for } i \neq j. \tag{2.6}$$

We will denote the common interfaces by $F_{ij} = \partial\Omega_i \cap \partial\Omega_j$, for $1 \leq i \neq j \leq N$, see Fig. 1(a). We use the notation $\mathcal{T}_H(\Omega) := \{\Omega_1, \Omega_2, \ldots, \Omega_N\}$ for the decomposition in (2.6). Having (2.6),

we can independently discretize the problem on the different patches Ω_i based on the geometry of each patch and the regularity properties of the solution. Essentially, the decomposition (2.6) helps us to consider N local problems posed on each patch, where interface conditions are used for coupling these local problems. Typically, the interface conditions across each F_{ij} are derived by a theoretical study of the elliptic problem (2.3) and concern continuity requirements of the solution, e.g.,

$$[\![u]\!] := u_i - u_j = 0 \text{ on } F_{ij}, \quad \text{and} \quad [\![\rho\nabla u]\!] \cdot n_{F_{ij}} := (\rho_i \nabla u_i - \rho_j \nabla u_j) \cdot n_{F_{ij}} = 0 \text{ on } F_{ij}, \tag{2.7}$$

where $n_{F_{ij}}$ is the unit normal vector on F_{ij} with direction towards Ω_j, and u_i denote the restriction of u to Ω_i. Using the decomposition $\mathcal{T}_H(\Omega)$ and the interface conditions (2.7), the variational equation (2.4) can be rewritten as

$$\sum_{i=1}^{N} \int_{\Omega_i} \rho_i(x) \nabla u \nabla \phi \, dx - \sum_{F_{ij}} \int_{F_{ij}} [\![\rho \nabla u \phi]\!] \cdot n_{F_{ij}} \, d\sigma = \sum_{i=1}^{N} \int_{\Omega_i} f\phi \, dx, \quad \text{for } \phi \in H_0^1(\Omega). \tag{2.8}$$

The dG schemes usually use numerical fluxes on every interface F_{ij} for imposing weakly the interface conditions (2.7) and for coupling the local problems, see, e.g., [11, 31, 32].
Let $\ell \geq 2$ be an integer, we define the broken Sobolev space

$$H^\ell(\mathcal{T}_H(\Omega)) = \{u \in L^2(\Omega) : u_i = u|_{\Omega_i} \in H^\ell(\Omega_i), \text{ for } i = 1, \ldots, N\}. \tag{2.9}$$

Assumption 1 *We assume that the solution u of (2.4) belongs to $V = H^1(\Omega) \cap H^\ell(\mathcal{T}_H(\Omega))$ with $\ell \geq 2$.*

Remark 1. For cases with high discontinuities of ρ, the solution u of (2.5) does not generally have the regularity properties of Assumption 1. We study dG IgA methods for these problems in [25].

2.4 B-spline spaces

In this section, we briefly present the B-spline spaces and the form of the B-spline parametrizations for the physical subdomains. For a better presentation of the B-spline space, we start our discussion for the one-dimensional case. Then we proceed to higher dimensions. We refer to [7], [10] and [34] for a more detailed presentation.

Consider, $\mathcal{Z} = \{0 = z_1, z_2, \cdots, z_M = 1\}$ to be a partition of $I = [0, 1]$ with $I_j = [z_j, z_{j+1}]$, $j = 1, \cdots, M-1$ to be the intervals of the partition. Let the integers p and n_1 denote the p spline degree and the number of the B-spline bases. Based on $\mathcal{Z}$, we introduce the knot vector $\Xi = \{0 = \xi_1 \leq \xi_2 \leq \ldots \leq \xi_{n_1+p+1} = 1\}$, where we allow repetitions of the knots, which are given by the associated vector $\mathcal{M} = \{m_1, \cdots, m_M\}$, that means,

$$\Xi = \{\underbrace{0 = \xi_1, \cdots \xi_{m_1}}_{=z_1}, \underbrace{\xi_{m_1+1} = \cdots = \xi_{m_1+m_2}}_{=z_2}, \cdots, \underbrace{\xi_{n_1+p+1-m_M}, \cdots, \xi_{n_1+p+1} = 1}_{=z_M}\}. \tag{2.10}$$

The B-spline basis functions are defined by the Cox-de Boor formula, see, e.g., [7] and [10],

$$B_{i,p} = \frac{x - \xi_i}{\xi_{i+p} - \xi_i} B_{i,p-1}(x) + \frac{\xi_{i+p+1} - x}{\xi_{i+p+1} - \xi_{i+1}} B_{i+1,p-1}(x), \tag{2.11}$$

$$\text{with } B_{i,0}(x) = \begin{cases} 1, \text{ if } \xi_i \leq x \leq \xi_{i+1}, \\ 0, \text{ otherwise} \end{cases}$$

We assume that $m_j \leq p$ for all internal knots, which in turn gives that, at z_j the B-spline basis have $\kappa_j = p - m_j$ continuous derivatives.

Let us now consider the unit cube $\widehat{\Omega} = (0,1)^d \subset \mathbb{R}^d$, which we will refer to as the parametric domain, and let Ω_i, $i = 1, \dots, N$, be a decomposition of Ω as given in (2.6). Let the integers p and n_k denote the given B-spline degree and the number of basis functions of the B-spline space that will be constructed in x_k-direction with $k = 1, \dots, d$. We introduce the $d-$dimensional vector of knots $\boldsymbol{\Xi}_i^d = (\Xi_i^1, \dots, \Xi_i^k, \dots, \Xi_i^d)$, $k = 1, \dots, d$, with the particular components given by $\Xi_i^k = \{0 = \xi_1^k \leq \xi_2^k \leq \dots \leq \xi_{n_k+p+1}^k = 1\}$. The components Ξ_i^k of $\boldsymbol{\Xi}_i^d$ form a mesh $T^{(i)}_{h_i,\widehat{\Omega}} = \{\hat{E}_m\}_{m=1}^{M_i}$ in $\widehat{\Omega}$, where $\hat{E}_m$ are the micro elements and h_i is the mesh size, which is defined as follows. Given a micro element $\hat{E}_m \in T^{(i)}_{h_i,\widehat{\Omega}}$, we set $h_{\hat{E}_m} = \operatorname{diam}(\hat{E}_m) = \max\limits_{x_1,x_2 \in \hat{E}_m} \|x_1 - x_2\|_d$, where $\|.\|_d$ is the Euclidean norm in $\mathbb{R}^d$. The subdomain mesh size h_i is defined to be $h_i = \max\{h_{\hat{E}_m}\}$. We set $h = \max\limits_{i=1,\dots,N}\{h_i\}$. We refer the reader to [7] for more information about the meaning of the knot vectors in CAD and IgA.

Assumption 2 *The meshes $T^{(i)}_{h_i,\widehat{\Omega}}$ are quasi-uniform, i.e., there exist a constant $\theta \geq 1$ such that $\theta^{-1} \leq h_{\hat{E}_m}/h_{\hat{E}_{m+1}} \leq \theta$. Also, we assume that $h_i \sim h_j$ for $1 \leq i \neq j \leq N$.*

Given the knot vector Ξ_i^k in every direction $k = 1, \dots, d$, we construct the associated univariate B-spline basis, $\hat{\mathbb{B}}_{\Xi_i^k,p} = \{\hat{B}^{(i)}_{1,k}(\hat{x}_k), \dots, \hat{B}^{(i)}_{n_k,k}(\hat{x}_k)\}$ using the Cox-de Boor recursion formula, see, e.g., [7] and [10] for more details. On the mesh $T^{(i)}_{h_i,\widehat{\Omega}}$, we define the multivariate B-spline space $\hat{\mathbb{B}}_{\boldsymbol{\Xi}_i^d,k}$ to be the tensor-product of the corresponding univariate $\hat{\mathbb{B}}_{\Xi_i^k,p}$ spaces. Accordingly, the B-spline basis of $\hat{\mathbb{B}}_{\boldsymbol{\Xi}_i^d,k}$ are defined by the tensor-product of the univariate B-spline basis functions, that is

$$\hat{\mathbb{B}}_{\boldsymbol{\Xi}_i^d,p} = \otimes_{k=1}^d \hat{\mathbb{B}}_{\Xi_i^k,p} = \operatorname{span}\{\hat{B}_j^{(i)}(\hat{x})\}_{j=1}^{n=n_1\cdot\dots\cdot n_k\cdot\dots\cdot n_d}, \tag{2.12}$$

where each $\hat{B}_j^{(i)}(\hat{x})$ has the form

$$\hat{B}_j^{(i)}(\hat{x}) = \hat{B}^{(i)}_{j_1}(\hat{x}_1) \cdot \dots \cdot \hat{B}^{(i)}_{j_k}(\hat{x}_k) \cdot \dots \cdot \hat{B}^{(i)}_{j_d}(\hat{x}_d), \text{ with } \hat{B}^{(i)}_{j_k}(\hat{x}_k) \in \hat{\mathbb{B}}_{\Xi_i^k,k}. \tag{2.13}$$

In IgA framework, each Ω_i is considered as an image of a B-spline, NURBS, etc., parametrization mapping. Given the B-spline spaces and having defined the control points $\mathbf{C}_j^{(i)}$, we parametrize each subdomain Ω_i by the mapping

$$\boldsymbol{\Phi}_i : \widehat{\Omega} \to \Omega_i, \quad x = \boldsymbol{\Phi}_i(\hat{x}) = \sum_{j=1}^{n} \mathbf{C}_j^{(i)} \hat{B}_j^{(i)}(\hat{x}) \in \Omega_i, \tag{2.14}$$

where $\hat{x} = \boldsymbol{\Phi}_i^{-1}(x)$, $i = 1, \dots, N$, cf. [7]. For every Ω_i, we construct a mesh $T^{(i)}_{h_i,\Omega_i} = \{E_m\}_{m=1}^{M_i}$, whose vertices are the images of the vertices of the corresponding parametric mesh $T^{(i)}_{h_i,\widehat{\Omega}}$ through $\boldsymbol{\Phi}_i$. For each Ω_i, $i = 1, \dots, N$, we construct the B-spline space $\mathbb{B}_{\boldsymbol{\Xi}_i^d,k}$ as

$$\mathbb{B}_{\boldsymbol{\Xi}_i^d,p} := \{B_j^{(i)}|_{\Omega_i} : B_j^{(i)}(x) = \hat{B}_j^{(i)} \circ \boldsymbol{\Phi}_i^{-1}(x), \text{ for } \hat{B}_j^{(i)} \in \hat{\mathbb{B}}_{\boldsymbol{\Xi}_i^d,p}\}. \tag{2.15}$$

The global B-spline space V_h with components on every $\mathbb{B}_{\boldsymbol{\Xi}_i^d,p}$ is defined by

$$V_h := \mathbb{B}_{\boldsymbol{\Xi}_1^d,p} + \dots + \mathbb{B}_{\boldsymbol{\Xi}_N^d,p} := V_{h_1}^{(1)} + \dots + V_{h_N}^{(N)}. \tag{2.16}$$

Remark 2. The B-spline spaces presented above are referred to the general case of N subdomains. As we point out in the previous subsection, the mappings in (2.14) should provide matching interface parametrizations. Throughout the paper we study the crime case where the mappings in (2.14) produce non-matching interface parametrizations.

Assumption 3 *Assume that every $\boldsymbol{\Phi}_i$, $i = 1, ..., N$ is sufficiently smooth and there exist constants $0 < c < C$ such that $c \leq |\det J_{\boldsymbol{\Phi}_i}| \leq C$, where $J_{\boldsymbol{\Phi}_i}$ is the Jacobian matrix of $\boldsymbol{\Phi}_i$.*

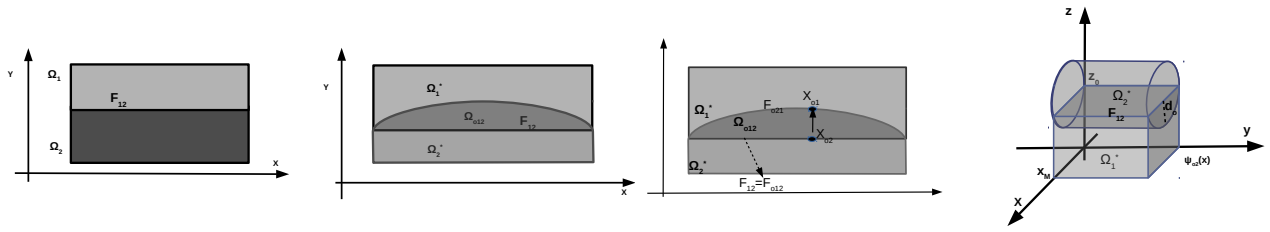

Fig. 1. (a) Illustration of a decomposition with matching interface paramtrizations, (b) an IgA decomposition including overlapping patches in 2d, (c) the locations of the diametrically opposite points on the overlapping boundaries, (d) an IgA decomposition including overlapping patches in 3d.

2.5 Non-matching parametrized interfaces

For increasing the flexibility of the IgA approach, we see Ω as a union of patches, see (2.6) and an illustration Fig. 1. In particular, for each patch $\overline{\Omega}_i$, $i = 1, \cdots, N$, we find the control net and then each patch has its parametrization, i.e., $\overline{\Omega}_i = \mathbf{\Phi}_i(\widehat{\Omega})$, see (2.14). Usually, the control points, which are related to the patch interfaces F_{ij}, are appropriately matched in order the parametrizations $\mathbf{\Phi}_i$ and $\mathbf{\Phi}_j$ of neighboring patches to give the same parametrized interface. However, in some cases, the control points of the adjacent points, may not be in correct correspondence. This can lead in the case where, the adjoint parametrizations are unable to provide identical parmetrizations for the (physical common) patch interfaces. We refer to this phenomena as non-matching interface parametrizations. The result of having non-matching interface parametrizations is the existence of gap and overlapping regions in the multi-patch representation of the domain. The main problem during the dG IgA procedure for solving the PDE problem on these type decompositions is the weakness of a direct use of the interface conditions (2.7), for constructing the numerical fluxes. For this we use appropriately modified dG IgA approaches. These type of methods have recently been presented in [17] and [19], for decompositions including gap regions and in [18] on decompositions with gaps and overlapping regions. In this work, we focus on the case of having decompositions with overlapping regions. We present a new error analysis, where the global approximation error is split into two parts. The first is coming by the approximation properties of the B-splines. The second is further split into a component related to the construction of artificial interface conditions on overlap boundaries, and into a second component which is related to a consistency error due to the coexistence of different diffusion coefficients, lets say ρ_i and ρ_j on the overlapping region $\Omega_i \cap \Omega_j$. The first part error will be estimated based on known interpolation estimates of the B-spline spaces, see e.g., [4], [8] and [25]. The second will be estimated following the same steps as in [17], [19] and [18]. For the estimation of the third error, we will follow ideas of Strang's Lemma, see [12]. We point out that the investigation of estimates for the third component error has not been presented in [18].

2.6 Overlapping regions

We now describe decompositions with overlapping regions. To simplify the description and to explain our ideas, we will consider a decomposition with two patches. Recalling (2.6), we suppose that there are two so called *physical* patches Ω_1 and Ω_2 that form a natural decomposition of Ω without overlapping regions, i.e.,

$$\overline{\Omega} = \overline{\Omega_1} \cup \overline{\Omega_2}, \quad \overline{\Omega_1} \cap \overline{\Omega_2} = \emptyset, \text{ with } F_{12} = \partial\Omega_1 \cap \partial\Omega_2, \tag{2.17}$$

where F_{12} is the physical interface. We consider the case where, after constructing the control nets for the two patches Ω_1 and Ω_2, the control points which are associated with the common physical interface F_{12} do not match appropriately, resulting in that way to non-matching interface parametrizations. Lets denote $\mathbf{\Phi}_1^* : \widehat{\Omega} \to \Omega_1^*$ and $\mathbf{\Phi}_2^* : \widehat{\Omega} \to \Omega_2^*$, the two produced parametrizations and let Ω_1^* and Ω_2^* be the two patches of the corresponding "in-correct" parametrizations. We denote the overlapping region by Ω_{o21}, i.e., $\Omega_{o21} = \Omega_1^* \cap \Omega_2^*$, and we assume that $\Omega = \Omega_1^* \cup \Omega_2^*$. We denote the interior boundary faces of the the overlapping region, by $F_{o12} = \partial\Omega_1^* \cap \Omega_2^*$ and $F_{o21} = \partial\Omega_2^* \cap \Omega_1^*$, which implies that $\partial\Omega_{o21} = F_{o12} \cup F_{o21}$. For a function u^* defined in Ω we denote the jump of u^* across the interfaces by $[\![u^*]\!]|_{F_{oij}} = u_i^* - u_j^*$, where $u_i^* = u^*|_{\Omega_i^*}$, $i = 1, 2$ is the restriction of u to Ω_i^*. Finally, let $n_{F_{oij}}$ denote the unit exterior normal vector to F_{oij}, for $i \neq j$, $i, j = 1, 2$. Without loss of generality, we make the following assumptions.

Assumption 4 *Let Ω_1 and Ω_2 be the subdomains of the physical decomposition. Let Ω_1^* and Ω_2^* be the associated patches formed under the incorrect parametrizations $\mathbf{\Phi}_1^*$ and $\mathbf{\Phi}_2^*$, respectively. We assume that:*
(a) Ω_1^* and Ω_2^* are quite smooth domains.
(b) The exterior boundary parts of $\partial\Omega_1^*$ and $\partial\Omega_2^*$ are subsets of $\partial\Omega$.
(c) $\Omega_2 \subset \overline{\Omega_2^*}$ and $\Omega_{o21} \cap \partial\Omega = \emptyset$.
(d) $\overline{\Omega_1} := \overline{\Omega_1^*}$, and the face F_{o12} coincides with the physical interface, i.e., $F_{o12} = F_{12}$.
(e) the face F_{o21} is a simple face and meaning that it can be described as the set of points (x, y, z) satisfying the inequalities

$$0 \leq x \leq x_{Mo},\ 0 \leq y \leq \psi_{o2}(x),\ z = z_0, \tag{2.18}$$

where x_{Mo} and z_0 are fixed real numbers, ψ_{o2} is a given smooth functions, see Figs. 1(b),(c),(d).

To proceed and to build up the auxiliary interface conditions on $\partial\Omega_{o21}$, we need to assign the points located on F_{o12} to the diametrically opposite points located on F_{o21}. Implicitly this means to find a convenient form to ψ_{o2} function and for its inverse. We construct a parametrization for the face F_{o21}, i.e., a mapping $\mathbf{\Phi}_{o12} : F_{o12} \to F_{o21}$, of the form

$$x_{o1} \in F_{o12} \to \mathbf{\Phi}_{o12}(x_{o1}) := x_{o2} \in F_{o21}, \quad \text{with} \quad \mathbf{\Phi}_{o12}(x_{o1}) = x_{o1} + \zeta_o(x_{o1}) n_{F_{o12}}, \tag{2.19}$$

where ζ_o is a B-spline and $n_{F_{o12}}$ is the unit normal vector on F_{o12}. Note that, we can construct the B-spline function ζ_o in (2.19), because the curve F_{o21} is a B-spline curve, precisely is the image of a part of $\partial\widehat{\Omega}$ under $\mathbf{\Phi}_2^*$, see also remarks in [18]. Utilizing the mapping $\mathbf{\Phi}_{o12}$ given in (2.19), we can consider each point $x_{o2} \in F_{o21}$ as an image by means of $\mathbf{\Phi}_{o12}$ of a point $x_{o1} \in F_{o12}$, see Fig. 1(c). Finally, we introduce a parameter d_o, which help us to quantify the width of the overlapping region Ω_{o21}

$$d_o = \max_{x_{o1} \in F_{o12}} |x_{o1} - \mathbf{\Phi}_{o12}(x_{o1})|. \tag{2.20}$$

We are interested in overlapping regions, where their width d_o decreases polynomially in h, i.e.,

$$d_o \leq h^\lambda, \quad \text{with some} \quad \lambda \geq 1. \tag{2.21}$$

Based on this, we assume that $n_{F_{o12}} \approx -n_{F_{o21}}$, and define the mapping $\mathbf{\Phi}_{o21} : F_{o21} \to F_{o12}$ as

$$\mathbf{\Phi}_{o21}(x_{o2}) = x_{o1}, \ \text{with} \quad \mathbf{\Phi}_{o12}(x_{o1}) = x_{o2}. \tag{2.22}$$

Essentially, $\mathbf{\Phi}_{o21}$ will play the role of the inverse of mapping $\mathbf{\Phi}_{o12}$. For detailed commends about the assumption $n_{F_{o12}} \approx -n_{F_{o21}}$ and the definition of $\mathbf{\Phi}_{o21}$, we refer to [17], [19], and [18].

Remark 3. In view of Assumption 4 and (2.19), we consider the following case: let F_{12} to be described as $F_{12} = \{(x, y) : 0 \leq x \leq 1,\ y = 0\}$. Then $F_{o21} = \{(x, y) : 0 \leq x \leq 1,\ 0 \leq y \leq \zeta_0(x)\}$ with $\|\zeta_0(x)\|_{L^\infty} = d_o \leq h^\lambda$. Then, the integral of a given function $f : \Omega \to \mathbb{R}$ over F_{o21}, is evaluated by $\int_{F_{o21}} f(x, y)\, ds = \int_0^1 f(x, \zeta_0(x))\sqrt{1 + (\zeta_0'(x))^2}\, dx$.

We deduce our results under the following convenient assumption.

Assumption 5 *We suppose that there exist an associated refinement of the knot vector $\boldsymbol{\Xi}_2^d$, such that the interface F_{o12} can be seen as an image of $\boldsymbol{\Phi}_2^*$, i.e., F_{o12} is an image under $\boldsymbol{\Phi}_2^*$ of a mesh line of $T^{(2)}_{h_2,\widehat{\Omega}}$. A schematic illustration is presented in Fig. 2.*

Note that the refined knot vector in Assumption 5 is related to the mesh for approximating the solution of the PDE problem and not to the control net.

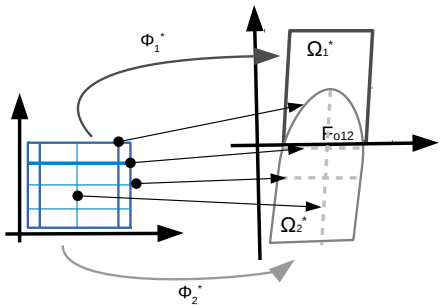

Fig. 2. The interface F_{o12} as an image of a parametric mesh-line under the $\boldsymbol{\Phi}_2^* : \widehat{\Omega} \to \Omega_2^*$.

2.7 $\boldsymbol{\Phi}_i^*$-directional derivatives

Following the results presented in [9, 8], we introduce in briefly the derivatives of a function f defined in Ω, with respect to the coordinate system that is naturally introduced by the mappings $\boldsymbol{\Phi}_i^* : \widehat{\Omega} \to \Omega_i^*$, $i = 1, 2$. Denote $\mathbf{g}_{i,j}(x) = \Big[\dfrac{\partial \Phi_{i,1}^*}{\partial x_j}(\boldsymbol{\Phi}_i^{*^{-1}}(x)), \cdots, \dfrac{\partial \Phi_{i,d}^*}{\partial x_j}(\boldsymbol{\Phi}_i^{*^{-1}}(x))\Big]$. The first order derivatives are just the directional derivatives with respect to $\mathbf{g}_{i,j}$, i.e.,

$$\frac{\partial f(x)}{\partial \mathbf{g}_{i,j}} = \nabla f(x) \cdot \mathbf{g}_{i,j}(x). \tag{2.23a}$$

The "one-directional" high-order derivatives are accordingly defined as

$$\frac{\partial^{\alpha_i} f}{\partial \mathbf{g}_{i,j}^{\alpha_i}} = \underbrace{\frac{\partial f}{\partial \mathbf{g}_{i,j}}\Big(\ldots\Big(\frac{\partial f}{\partial \mathbf{g}_{i,j}}\Big)\Big)}_{\alpha_i - times}. \tag{2.23b}$$

For multi-direction derivatives, we use the notation

$$D^{\boldsymbol{\alpha}}_{\boldsymbol{\Phi}_i^*} f = \frac{\partial^{\alpha_1} f}{\partial \mathbf{g}_{n,1}} \cdots \frac{\partial^{\alpha_d} f}{\partial \mathbf{g}_{n,d}}. \tag{2.23c}$$

In relation to the $D^{\boldsymbol{\alpha}}_{\boldsymbol{\Phi}_i^*} f$ derivatives, we define the norms and seminorms

$$\|f\|^2_{\mathcal{H}^{\boldsymbol{\alpha}}_{\boldsymbol{\Phi}^*_i}(\Omega^*_i)} = \sum_{s_1=0}^{\alpha_1} \cdots \sum_{s_d=0}^{\alpha_d} |f|^2_{\mathcal{H}^{\boldsymbol{\alpha}}_{\boldsymbol{\Phi}^*_i}(\Omega^*_i)}, \qquad |f|^2_{\mathcal{H}^{\boldsymbol{\alpha}}_{\boldsymbol{\Phi}^*_i}(\Omega^*_i)} = \sum_{E \in T^{(i)}_{h_i,\Omega^*_i}} |f|^2_{H^{\boldsymbol{\alpha}}_{\boldsymbol{\Phi}^*_i}(E)}, \tag{2.24}$$

$$\text{where} \quad |f|^2_{H^{\boldsymbol{\alpha}}_{\boldsymbol{\Phi}^*_i}(E)} = \|D^{\boldsymbol{\alpha}}_{\boldsymbol{\Phi}^*_i} f\|_{L^2(E)}.$$

We introduce the space $H^{\boldsymbol{\alpha}}_{\boldsymbol{\Phi}^*_i}(\Omega^*_i)$ endowed with the norm $\|\cdot\|_{H^{\boldsymbol{\alpha}}_{\boldsymbol{\Phi}^*_i}(\Omega^*_i)} = \|\cdot\|_{\mathcal{H}^{\boldsymbol{\alpha}}_{\boldsymbol{\Phi}^*_i}(\Omega^*_i)}$.

3 The patch-wise problems and the modified fluxes

The main goal is to give an estimate for the difference between the solution u defined in (2.4), computed on the physical decomposition (2.17), and the dG IgA solution u^*_h, which is computed on the incorrect decomposition $\mathcal{T}^*_H = \overline{\Omega^*_1} \cup \overline{\Omega^*_2}$. The incompatibility between the $\mathcal{T}_H$ and $\mathcal{T}^*_H$ and in particular the overlapping nature of $\mathcal{T}^*_H$ causes further difficulties. Namely, the local B-spline spaces of V_h in (2.16) are defined in correspondence to $\mathcal{T}^*_H$, and therefore on Ω_{o21} we have two different B-spline spaces, which will produce two different numerical solutions. Furthermore, on Ω_{o21} we have the overlapping of diffusion coefficients ρ_1 and ρ_2. For example, when we work on patch Ω^*_1 then we prefer setting $\rho := \rho_1$ in Ω_{o21} and conversely, when we work on Ω^*_2 we prefer setting $\rho := \rho_2$ in Ω_{o21}.

The patch-wise variational problems Let $\ell \geq 1$ be an integer. Accordingly to the space definitions (2.9), we introduce the spaces

$$\begin{aligned} H^\ell(\mathcal{T}^*_H(\Omega_i)) :=& \{\{u^*_i\}^2_{i=1} : u^*_i \in H^\ell(\Omega^*_i), \text{ for } i = 1, 2\}, \\ H^\ell_0(\mathcal{T}^*_H(\Omega_i)) :=& \{\{u^*_i\}^2_{i=1} : u^*_i \in H^\ell_0(\Omega^*_i), \text{ for } i = 1, 2\}. \end{aligned} \tag{3.1}$$

For simplicity below, instead of writing $\{v^*_i\}^2_{i=1} \in H^\ell(\mathcal{T}^*_H(\Omega_i))$, we will write $v^* \in H^\ell(\mathcal{T}^*_H(\Omega_i))$. We recall the shape assumptions for Ω^*_1 and Ω^*_2, e.g see Assumption 4. Lets suppose for the moment that the traces $u|_{F_{o21}}$ and $u|_{F_{o12}}$ of the exact solution u are known and available. Then we consider the variational problems: for find $u, u^*_2 \in H^1(\Omega^*_2)$ such that

$$u^*_1 = u_D \text{ on } \partial\Omega^*_1 \cap \partial\Omega, \text{ and } u^*_1 = u|_{F_{o12}}, \; a^*_1(u^*_1, \phi_1) = l^*_1 f(\phi_1), \text{ for every } \phi_1 \in H^1_0(\Omega^*_1), \tag{3.2a}$$

where

$$a^*_1(u^*_1, \phi_1) = \int_{\Omega^*_1} \rho_1 \nabla u^*_1 \cdot \nabla \phi_1 \, dx - \int_{F_{o12}} \rho_1 \nabla u^*_1 \cdot n_{F_{o12}} \phi_1 \, d\sigma - \int_{\partial\Omega^*_1 \cap \partial\Omega} \rho_1 \nabla u^*_1 \cdot n_{\partial_{\Omega_1}} \phi_1 \, d\sigma, \tag{3.2b}$$

$$l^*_1 f(\phi_1) = \int_{\Omega^*_1} f \phi_1 \, dx, \tag{3.2c}$$

and

$$u^*_2 = u_D \text{ on } \partial\Omega^*_2 \cap \partial\Omega, \text{ and } u^*_2 = u|_{F_{o21}}, \; a^*_2(u^*_2, \phi_2) = l^*_2 f(\phi_2), \text{ for every } \phi_2 \in H^1_0(\Omega^*_2), \tag{3.2d}$$

where

$$a^*_2(u^*_2, \phi_2) = \int_{\Omega^*_2} \rho_2 \nabla u^*_2 \cdot \nabla \phi_2 \, dx - \int_{F_{o21}} \rho_2 \nabla u^*_2 \phi_2 \cdot n_{F_{o21}} \, d\sigma - \int_{\partial\Omega^*_2 \cap \partial\Omega} \rho_2 \nabla u^*_2 \cdot n_{\partial\Omega_2} \phi_2 \, d\sigma, \tag{3.2e}$$

$$l^*_2 f(\phi_2) = \int_{\Omega^*_2} f \phi_2 \, dx, \tag{3.2f}$$

and

$$u_{o,2} = u_D \text{ on } \partial\Omega_2^* \cap \partial\Omega, \text{and } u_{o,2} = u_{F_{o21}},\ a_{o,2}(u,\phi_2) = l_2^* f(\phi_2),\ \text{for every } \phi_2 \in H_0^1(\Omega_2^*), \quad (3.2g)$$

where

$$a_{o,2}(u_{o,2},\phi_2) = \int_{\Omega_{o21}} \rho_1 \nabla u_{o,2}\cdot\nabla\phi_2\,dx + \int_{\Omega_2} \rho_2 \nabla u_{o,2}\cdot\nabla\phi_2\,dx \quad (3.2h)$$
$$- \int_{F_{o21}} \rho_1 \nabla u_{o,2}\cdot n_{F_{o21}}\phi_2\,d\sigma - \int_{\partial\Omega_2^*\cap\partial\Omega} \rho_2 \nabla u_2^*\cdot n_{\partial\Omega_2}\phi_2\,d\sigma,$$
$$l_2^* f(\phi_2) = \int_{\Omega_2^*} f\phi_2\,dx. \quad (3.2i)$$

Note that the solution u of (2.5) satisfies (3.2a). Also, the restriction of the solution u of (2.5) to Ω_2^* satisfies the problems (3.2g), i.e., in this sense problem (3.2g) is consistent with (2.5). Thus, we write below u instead of $u_{o,2}$. In correspondence with Assumption 1, we make the assumption.

Assumption 6 *We suppose that the solutions of (3.2) belong to $H^\ell(\mathcal{T}_H^*(\Omega_i))$ with $\ell \geq 2$.*

Remark 4. We point out that, we derived the variational problems in (3.2) using the data and the properties of the solution u of (2.4). The problems in (3.2) can be considered as auxiliary perturbations of (2.4) compatible to $\mathcal{T}_H^*$. We do not investigate the well posedness of (3.2).

In order to proceed with our analysis, we first define the dG-norm $\|.\|_{dG}$ associated with $\mathcal{T}_H^*(\Omega)$. For all $v \in V_h^* := H^\ell(\mathcal{T}_H^*(\Omega_i)) + V_h$,

$$\|v\|_{dG}^2 = \sum_{i=1}^{2}\Big(\rho_i\|\nabla v_i\|_{L^2(\Omega_i^*)}^2 + \frac{\rho_i}{h}\|v_i\|_{L^2(\partial\Omega_i^*\cap\partial\Omega)}^2 + \sum_{F_{oij}\subset\partial\Omega_i^*}\frac{\{\rho\}}{h}\|v_i\|_{L^2(F_{oij})}^2\Big), \quad (3.3)$$

where F_{oij} with $1 \leq i \neq j \leq 2$ are the interior faces related to overlapping regions, see Fig. 1(b).

3.1 The consistency error.

The restriction of the solution u defined in (2.5) to Ω_2^* does not satisfy the local problem (3.2d). Comparing the problems (3.2g) and (3.2d), we can roughly say that there is an extra term $-(\rho_2-\rho_1)\nabla u_2^*$ in Ω_{o21}, which can be characterized as a non consistency term. We derive below a bound for this term.
Let $\phi \in H_0^1(\Omega_2^*)$. By a simple computations on the forms in (3.2), we have that

$$a_2^*(u_2^*,\phi_h) = \int_{\Omega_{o21}} \rho_1\nabla u_2^*\cdot\nabla\phi\,dx + \int_{\Omega_2}\rho_2\nabla u_2^*\cdot\nabla\phi\,dx - \int_{\partial\Omega_2\cap\partial\Omega}\rho_2\nabla u_2^*\cdot n_{\partial\Omega_2}\phi\,d\sigma$$
$$- \int_{F_{o21}}\rho_2\nabla u_2^*\cdot n_{F_{o21}}\phi\,d\sigma = \int_{\Omega_{o21}}(\rho_1-\rho_2)\nabla u_2^*\cdot\nabla\phi\,dx + l_2^* f(\phi). \quad (3.4)$$

On the other hand, under the Assumption 1, we immediately have that

$$a_{o,2}(u,\phi_2) = \int_{\Omega_{o21}}\rho_1\nabla u\cdot\nabla\phi\,dx + \int_{\Omega_2}\rho_2\nabla u\cdot\nabla\phi\,dx \quad (3.5)$$
$$- \int_{F_{o21}}\rho_1\nabla u\cdot n_{F_{o21}}\phi\,d\sigma - \int_{\partial\Omega_2^*\cap\partial\Omega}\rho_2\nabla u\cdot n_{\partial\Omega_2}\phi\,d\sigma = l_2^* f(\phi).$$

Subtracting (3.5) from (3.4) and using $\phi|_{\partial\Omega_2^*} = 0$ we obtain

$$\int_{\Omega_{o21}} \rho_1 \nabla(u_2^* - u) \cdot \nabla\phi \, dx + \int_{\Omega_2} \rho_2 \nabla(u_2^* - u) \cdot \nabla\phi \, dx = \int_{\Omega_{o21}} (\rho_1 - \rho_2) \nabla u_2^* \cdot \nabla\phi \, dx. \tag{3.6}$$

Applying integration by parts on the right hand side in (3.6) and then setting $\phi = u_2^* - u$, we derive that

$$\begin{aligned}
\int_{\Omega_2^*} \rho |\nabla(u_2^* - u)|^2 \, dx &= c_\rho \Big(- \int_{\Omega_{o21}} \rho_2 \Delta u_2^* (u_2^* - u) \, dx + \int_{F_{o12}} \rho_2 \nabla u_2^* \cdot n_{F_{o12}} (u_2^* - u) \, d\sigma \Big) \\
&\leq c_\rho \Big(\int_{\Omega_{o21}} f \, (u_2^* - u) \, dx + \int_{F_{o12}} \rho_2 \nabla u_2^* \cdot n_{F_{o12}} (u_2^* - u) \, d\sigma \Big) \\
&\overset{(2.1)}{\leq} c_\rho \|f\|_{L^2(\Omega_{o21})} \|u_2^* - u\|_{L^2(\Omega_{o21})} + \|\rho_2 \nabla u_2^*\|_{L^2(F_{o12})} \|u_2^* - u\|_{L^2(F_{o12})} \\
&\overset{(2.2)}{\leq} c_\rho \|f\|_{L^2(\Omega_{o21})} \, \|u_2^* - u\|_{L^2(\Omega_{o21})} + \|\rho_2 \nabla u_2^*\|_{L^2(F_{o12})} \|u_2^* - u\|^{\frac{1}{2}}_{L^2(\Omega_{o21})} \|u_2^* - u\|^{\frac{1}{2}}_{H^1(\Omega_{o21})} \\
&\overset{(2.2)}{\leq} c_1 \Big(\|f\|_{L^2(\Omega_{o21})} \, d_o \|\nabla(u_2^* - u)\|_{L^2(\Omega_{o21})} \\
&\quad + \|\rho_2 \nabla u_2^*\|_{L^2(F_{o12})} \, d_o^{\frac{1}{2}} \|\nabla(u_2^* - u)\|^{\frac{1}{2}}_{L^2(\Omega_{o21})} (d_o + 1) \|\nabla(u_2^* - u)\|^{\frac{1}{2}}_{L^2(\Omega_{o21})} \\
&\leq c_2 \Big(\|f\|_{L^2(\Omega_{o21})} + \|\rho_2 \nabla u_2^*\|_{L^2(F_{o12})} \Big) \, d_o^{\frac{1}{2}} \|\nabla(u_2^* - u)\|_{L^2(\Omega_{o21})},
\end{aligned} \tag{3.7}$$

where we have used that $0 < d_o < 1$. By (3.7), we can easily obtain that

$$\|\rho \nabla(u_2^* - u)\|_{L^2(\Omega_2^*)} \leq c_2 \, d_o^{\frac{1}{2}} \Big(\|f\|_{L^2(\Omega_{o21})} + \|\rho_2 \nabla u_2^*\|_{L^2(F_{o12})} \Big), \tag{3.8}$$

and this gives an estimate of the difference between the physical solution u and the perturbed solution u^*.

Now, let $\phi_h \in V_h$ and $w \in H^{\ell \geq 2}(\Omega_2^*)$. Utilizing that $[\![\rho \nabla w]\!]|_{F_{12}} \cdot n = 0$, we rewrite $a_2^*(\cdot, \cdot)$ defined in (3.2e) in a patch wise way using $a_{o,2}(\cdot, \cdot)$ defined in (3.2h), as follows

$$\begin{aligned}
a_2^*(w, \phi_h) = &\int_{\Omega_{o21}} \rho_1 \nabla w \cdot \nabla \phi_h \, dx + \int_{\Omega_2} \rho_2 \nabla w \cdot \nabla \phi_h \, dx - \int_{\partial\Omega_2 \cap \partial\Omega} \rho_2 \nabla w \cdot n_{\partial\Omega_2} \phi_h \, d\sigma \\
&- \int_{F_{o21}} \rho_1 \nabla w \cdot n_{F_{o21}} \phi_h \, d\sigma - \int_{F_{12}} (\rho_1 - \rho_2) \nabla w \cdot n_{F_{21}} \phi_h \, d\sigma \\
&+ \int_{\Omega_{o21}} (\rho_2 - \rho_1) \nabla w \cdot \nabla \phi_h \, dx - \int_{F_{12}} (\rho_2 - \rho_1) \nabla w \cdot n_{F_{21}} \, d\sigma - \int_{F_{o21}} (\rho_2 - \rho_1) \nabla w \cdot n_{F_{o21}} \phi_h \, d\sigma \\
= &a_{o,2}(w, \phi_h) + a_{res}(w, \phi_h),
\end{aligned} \tag{3.9}$$

where we defined

$$\begin{aligned}
a_{res}(w, \phi_h) = &\int_{\Omega_{o21}} (\rho_2 - \rho_1) \nabla w \cdot \nabla \phi_h \, dx - \int_{F_{12}} (\rho_2 - \rho_1) \nabla w \cdot n_{F_{21}} \, \phi_h \, d\sigma \\
&- \int_{F_{o21}} (\rho_2 - \rho_1) \nabla w \cdot n_{F_{o21}} \phi_h \, d\sigma.
\end{aligned} \tag{3.10}$$

By a simple application of divergence theorem we get

$$a_{res}(w, \phi_h) = \int_{\Omega_{o21}} -\mathrm{div}\big((\rho_2 - \rho_1) \nabla w \big) \phi_h \, dx. \tag{3.11}$$

Replacing w by u_2^* in (3.9) and (3.11) and then by problem (3.2e), we can infer that

$$a_2^*(u_2^*, \phi_h) = a_{o,2}(u_2^*, \phi_h) + \int_{\Omega_{o21}} -\mathrm{div}\big((\rho_2 - \rho_1) \nabla u_2^* \big) \phi_h \, dx = a_{o,2}(u_2^*, \phi_h) + \int_{\Omega_{o21}} \frac{(\rho_2 - \rho_1)}{\rho_1} f \, \phi_h \, dx. \tag{3.12}$$

Proposition 1. *Let $\phi_h \in V_h$. There is a $c > 0$ dependent on ρ but independent of u and Ω_{o21} such that*

$$\|\phi_h\|^2_{L^2(\Omega_{o21})} \leq c d_o\, h\Big(\int_{\Omega_2^*} |\nabla \phi_h|^2\, dx + \frac{\{\rho\}}{h} \int_{F_{o21}} \phi_h^2\, d\sigma.\Big) \tag{3.13}$$

Proof. Let $\mathbf{v} = (0, y\phi_h^2)$. Divergence theorem for $\mathbf{v}$ on Ω_{o21} and Remark 3 yield,

$$\int_{\Omega_{o21}} \phi_h^2\, dx + \int_{\Omega_{o21}} 2y\phi_h\, \partial_y \phi_h\, dx = \int_{F_{o21}} y\phi_h^2\, d\sigma. \tag{3.14}$$

Using that $y \leq d_o$ and applying (2.1) in (3.14) we obtain

$$\|\phi_h\|^2_{L^2(\Omega_{o21})} \leq \big(\epsilon^2 \int_{\Omega_{o21}} \phi_h^2\, dx + \frac{4}{\epsilon^2} \int_{\Omega_{o21}} d_o^2\, |\nabla \phi_h|^2\, dx + d_o h \frac{1}{h} \int_{F_{o21}} \phi_h^2\, d\sigma\big) \tag{3.15}$$

Gathering similar terms and choosing ϵ appropriately small, we get

$$c_{1,\epsilon} \|\phi_h\|^2_{L^2(\Omega_{o21})} \leq c_{2,\epsilon} c_\rho\, d_o h\Big(\int_{\Omega_2^*} \rho_2 |\nabla \phi_h|^2\, dx + \frac{\{\rho\}}{h} \int_{F_{o21}} \phi_h^2\, d\sigma\Big), \tag{3.16}$$

where we used that $d_o^2 \leq d_o h$. Rearranging appropriately the constants in (3.16) yields (3.13). ■

Corollary 1. *Let $f \in L^\infty(\Omega)$ and $\phi_h \in V_h^2$. There is a constant $c > 0$ dependent on F_{o21} but independent of h such that*

$$\int_{\Omega_{o21}} f\phi_h\, dx \leq c d_o\, \|f\|_{L^\infty(\Omega_{o21})} \|\phi_h\|_{dG}. \tag{3.17}$$

Proof. It follows by from the Cauchy-Schwartz inequality that

$$\int_{\Omega_{o21}} f\phi_h\, dx \leq \|f\|_{L^2(\Omega_{o21})} \|\phi_h\|_{L^2(\Omega_{o21})} \leq c_{F_o 21} d_o^{\frac{1}{2}} \|f\|_{L^\infty(\Omega_{o21})} \|\phi_h\|_{L^2(\Omega_{o21})}. \tag{3.18}$$

Using (3.13) in (3.18), the required assertion follows easily. ■

Remark 5. Alternatively to the previous analysis, we can use the trace inequality (2.2). Using (2.2) in (3.15) and applying (2.1), we get

$$\begin{aligned} \|\phi_h\|^2_{L^2(\Omega_{o21})} \leq \epsilon^2 \|\phi_h\|^2_{L^2(\Omega_{o21})} + \frac{4}{\epsilon^2} d_o^2 \|\nabla \phi_h\|^2_{L^2(\Omega_{o21})} + \\ C\big(\frac{d_o}{2} \|\phi_h\|^2_{L^2(\Omega_{o21})} + \frac{d_o}{2} \|\phi\|^2_{L^2(\Omega_{o21})} + \frac{d_o}{2} \|\nabla \phi_h\|^2_{L^2(\Omega_{o21})}\big). \end{aligned} \tag{3.19}$$

Now, choosing in (3.19) $\epsilon = \dfrac{1}{4}$ and mesh size such that $C d_o < \dfrac{1}{2}$, we can obtain the estimate

$$\|\phi_h\|^2_{L^2(\Omega_{o21})} \leq C_0 \frac{4}{\epsilon^2} d_o^2 \|\nabla \phi_h\|^2_{L^2(\Omega_{o21})}. \tag{3.20}$$

In this case, we can derive (3.17) assuming $f \in L^2(\Omega)$.

3.2 Modification of the fluxes using Taylor expansions.

Under the assumptions on problems (3.2), and Assumption 6, we can derive interface conditions similar to (2.7), e.g.,

$$\rho_1 \nabla u_1^* \cdot n_{F_{o21}} = \rho_2 \nabla u_2^* \cdot n_{F_{o21}}, \text{ and } (u_1^* - u_2^*) = 0, \text{on } F_{o21}. \tag{3.21}$$

Across F_{o12}, similar interface conditions are not known. Hence, we derive below approximations of the jumps of the fluxes across F_{o12}. We use these approximations to appropriately modify the fluxes in (3.2) in order to couple the local problems (3.2a) and (3.2d).

Let $x, y \in \overline{\Omega}_2^*$ and let $f \in C^{m\geq 2}(\overline{\Omega}_2^*)$. We recall Taylor's formula with integral remainder

$$f(y) = f(x) + \nabla f(x) \cdot (y - x) + R^2 f(y + s(x - y)), \tag{3.22a}$$
$$f(x) = f(y) - \nabla f(y) \cdot (y - x) + R^2 f(x + s(y - x)), \tag{3.22b}$$

where $R^2 f(y + s(x - y))$ and $R^2 f(x + s(y - x))$ are the second order remainder terms defined by

$$R^2 f(y + s(x - y)) = \sum_{|\alpha|=2} (y - x)^\alpha \frac{2}{\alpha!} \int_0^1 s D^\alpha f(y + s(x - y))\, ds, \tag{3.23a}$$
$$R^2 f(x + s(y - x)) = \sum_{|\alpha|=2} (x - y)^\alpha \frac{2}{\alpha!} \int_0^1 s D^\alpha f(x + s(y - x))\, ds. \tag{3.23b}$$

By (3.22) it follows that

$$\nabla f(y) \cdot (y - x) = \nabla f(x) \cdot (y - x) + \big(R^2 f(x + s(y - x)) + R^2 f(y + s(x - y))\big), \tag{3.24a}$$
$$-f(x) = -f(y) + \nabla f(x) \cdot (y - x) + R^2 f(y + s(x - y)). \tag{3.24b}$$

Let $x_{o1} \in F_{o12}$ and $x_{o2} \in F_{o21}$ be such that $x_{o1} = \mathbf{\Phi}_{o21}(x_{o2})$. These will play the role of the points x and y in (3.22). Denoting $r_{o12} = x_{o1} - x_{o2}$ and using the assumption that $r_{o12} = -r_{o21}$, see Section 2.6 and (2.19) and (2.22), we obtain that $n_{F_{o12}} = \dfrac{r_{o12}}{|r_{o12}|} = -n_{F_{o21}}$.

For simplifying formulas, let us denote $R^2 u^*_{x_{o1}} := R^2 u^*(x_{o1} + s(x_{o2} - x_{o1}))$ and $R^2 u^*_{x_{o2}} := R^2 u^*(x_{o2} + s(x_{o1} - x_{o2}))$. Using the expansions (3.24) and interface conditions (3.21), we can modify the fluxes in forms given in (3.2b) and (3.2e) as follows,

$$\begin{aligned}
\int_{F_{o21}} \rho_2 \nabla u_2^*(x_{o2}) \cdot n_{F_{o21}} \phi \, d\sigma &= \int_{F_{o21}} \frac{1}{2}\big(\rho_2 \nabla u_2^*(x_{o2}) \cdot n_{F_{o21}} + \rho_1 \nabla u_1^*(x_{o2}) \cdot n_{F_{o21}}\big)\phi \, d\sigma \\
&= \int_{F_{o21}} \frac{1}{2}\big(\rho_2 \nabla u_2^*(x_{o2}) + \rho_1 \nabla u_1^*(\mathbf{\Phi}_{o21}(x_{o2})) \cdot n_{F_{o21}}\big)\phi + \big(R^2 u^*_{x_{o1}} + R^2 u^*_{x_{o2}}\big)\phi \, d\sigma \\
&\quad - \int_{F_{o21}} \frac{\{\rho\}}{h}(u_2^*(x_{o2}) - u_2^*(\mathbf{\Phi}_{o21}(x_{o2}))\phi + \frac{\{\rho\}}{h}\big(|r_{o12}| \nabla u_2^*(x_{o2}) \cdot n_{F_{o21}} + R^2 u^*_{x_{o2}}\big)\phi \, d\sigma,
\end{aligned} \tag{3.25a}$$

where $\{\rho\} = \dfrac{1}{2}(\rho_1 + \rho_2)$ and note that the last integral is equal to zero. Similarly we can have

$$\begin{aligned}
\int_{F_{o12}} \rho_1 \nabla u_1^*(x_{o1}) \cdot n_{F_{o12}} \phi \, d\sigma &= \int_{F_{o12}} \frac{1}{2}\big(\rho_2 \nabla u_2^*(\mathbf{\Phi}_{o12}(x_{o1})) + \rho_1 \nabla u_1^*(x_{o1}) \cdot n_{F_{o12}}\big)\phi + \big(R^2 u^*_{x_{o2}} + R^2 u^*_{x_{o1}}\big)\phi \, d\sigma \\
&\quad - \int_{F_{o12}} \frac{\{\rho\}}{h}(u_2^*(\mathbf{\Phi}_{o12}(x_{o1})) - u_1^*(x_{o1})\phi + \frac{\{\rho\}}{h}\big(|r_{o21}| \nabla u_1^*(x_{o1}) \cdot n_{F_{o12}} + R^2 u^*_{x_{o1}}\big)\phi \, d\sigma.
\end{aligned} \tag{3.25b}$$

3.3 The discrete problem

The global modified form To treat the overlapping nature of the IgA parametrizations, we consider a global bilinear form $a^*(\cdot,\cdot)$ formed by the contributions of $a_i^*(\cdot,\cdot)$, $i=1,2$ given in (3.2a) and (3.2d). We replace the flux forms of $a_i^*(\cdot,\cdot)$ by the flux forms given in (3.25). Let $\phi_h=(\phi_{1h},\phi_{2h})\in V_h$, by adding $a_1^*(\cdot,\cdot)+a_1^*(\cdot,\cdot)$, we successively get

$$
\begin{aligned}
a^*(u^*,\phi_h)=a_2^*(u_2^*,\phi_h)+a_1^*(u_1^*,\phi_h)&=\int_{\Omega_1^*}\rho_1\nabla u_1^*\cdot\nabla\phi_{1h}\,dx+\int_{\Omega_2^*}\rho_2\nabla u_2^*\cdot\nabla\phi_{2h}\,dx\\
&-\int_{\partial\Omega_1^*\cap\partial\Omega}\rho_1\nabla u_1^*\cdot n_{\partial\Omega_1^*}\phi_{1h}\,d\sigma-\int_{\partial\Omega_2^*\cap\partial\Omega}\rho_2\nabla u_2^*\cdot n_{\partial\Omega_2^*}\phi_{2h}\,d\sigma\\
&+\frac{\rho_1}{h}\int_{\partial\Omega_1^*\cap\partial\Omega}(u_1^*-u_D)\phi_{1h}\,d\sigma+\frac{\rho_2}{h}\int_{\partial\Omega_2^*\cap\partial\Omega}(u_2^*-u_D)\phi_{1h}\,d\sigma\\
-\int_{F_{o12}}\frac{1}{2}\big(\rho_2\nabla u_2^*(\boldsymbol{\Phi}_{o12}(x_{o1}))+\rho_1\nabla u_1^*(x_{o1})\big)\cdot n_{F_{o12}}&++\frac{\{\rho\}}{h}(u_2^*(\boldsymbol{\Phi}_{o12}(x_{o1}))-u_1^*(x_{o1})\phi_{1h}\,d\sigma\\
-\int_{F_{o21}}\frac{1}{2}\big(\rho_2\nabla u_2^*(x_{o2})+\rho_1\nabla u_1^*(\boldsymbol{\Phi}_{o21}(x_{o2}))\big)\cdot n_{F_{o21}}&+\frac{\{\rho\}}{h}(u_2^*(x_{o2})-u_2^*(\boldsymbol{\Phi}_{o21}(x_{o2}))\phi_{2h}\,d\sigma\\
&+\int_{F_{o21}}\big(R^2u_{x_{o1}}^*+R^2u_{x_{o2}}^*\big)-\frac{\{\rho\}}{h}\big(|r_{o12}|\nabla u_2^*(x_{o2})\cdot n_{F_{o21}}+R^2u_{x_{o2}}^*\big)\phi_{2h}\,d\sigma\\
&+\int_{F_{o12}}\big(R^2u_{x_{o2}}^*+R^2u_{x_{o1}}^*\big)-\frac{\{\rho\}}{h}\big(|r_{o21}|\nabla u_1^*(x_{o1})\cdot n_{F_{o12}}+R^2u_{x_{o1}}^*\big)\phi_{1h}\,d\sigma\\
&=\int_{\Omega_1^*}f\phi_{1h}\,dx+\int_{\Omega_2^*}f\phi_{2h}\,dx. \quad (3.26)
\end{aligned}
$$

Remark 6. The previous form (3.26) is referred to the perturbed solution u^*. Since the exact solution u hasd the same regularity properties, see Assumption 1, we can derive analogous formulation as in (3.26) for u. Using (3.2), (3.9), we can show that

$$
a_1^*(u,\phi_h)+a_{o,2}^*(u,\phi_h)=a^*(u,\phi_h)-a_{res}(u,\phi_h)=\int_{\Omega_1^*}f\phi_{1h}\,dx+\int_{\Omega_2^*}f\phi_{2h}\,dx, \tag{3.27}
$$

The dG IgA scheme. In view of (3.26), we define the forms $A_{\Omega_i^*}(\cdot,\cdot):V_h^*\times V_h\to\mathbb{R}$, $R_{\Omega_{o21}}(\cdot,\cdot):V_h^*\times V_h\to\mathbb{R}$, and the linear functional and the linear functional $l_{f,\Omega_i^*}:V_h\to\mathbb{R}$ by

$$
\begin{aligned}
A_{\Omega_i^*}(u^*,\phi_h)=\sum_{i=1}^{2}\Big(&\int_{\Omega_i^*}\rho_i\nabla u_i^*\cdot\nabla\phi_h\,dx-\int_{\partial\Omega_i^*\cap\partial\Omega}\rho_i\nabla u_i^*\cdot n_{\partial\Omega_i^*}\phi_h\,d\sigma \qquad (3.28a)\\
&-\sum_{F_{oij}\subset\partial\Omega_i^*}\int_{F_{oij}}\big\{\rho_i\nabla u_i^*\big\}\cdot n_{F_{oij}}\phi_h-\frac{\eta\{\rho\}}{h}\big(u_i^*-u_j^*\big)\phi_h\,d\sigma\Big),\ 1\le i\ne j\le 2,
\end{aligned}
$$

$$
\begin{aligned}
R_{\Omega_{o21}}(u^*,\phi_h)=&\int_{F_{o21}}\big(R^2u_{x_{o1}}^*+R^2u_{x_{o2}}^*\big)-\frac{\{\rho\}}{h}\big(|r_{o12}|\nabla u_2^*(x_{o2})\cdot n_{F_{o21}}+R^2u_{x_{o2}}^*\big)\phi_h\,d\sigma\\
&+\int_{F_{o12}}\big(R^2u_{x_{o2}}^*+R^2u_{x_{o1}}^*\big)-\frac{\{\rho\}}{h}\big(|r_{o21}|\nabla u_1^*(x_{o1})\cdot n_{F_{o12}}+R^2u_{x_{o1}}^*\big)\phi_h\,d\sigma \qquad (3.28b)\\
l_{f,\Omega_i^*}(\phi_h)=&\sum_{i=1}^{N}\int_{\Omega_i^*}f\phi_h\,dx,
\end{aligned}
$$

where $\eta > 0$ is a parameter that is introduced for establishing the coercivity of the resulting dG bilinear form on the IgA spaces V_h. Based on (3.26) an the forms defined in (3.28) we introduce the discrete bilinear form $A_h(\cdot,\cdot) : V_h \times V_h \to \mathbb{R}$ and the linear form $F_h : V_h \to \mathbb{R}$ as follows

$$A_h(u_h^*, \phi_h) = A_{\Omega_i^*}(u_h^*, \phi_h) + \sum_{i=1}^{2} \frac{\eta\rho_i}{h} \int_{\partial\Omega_i^* \cap \partial\Omega} u_h^* \phi_h \, d\sigma, \tag{3.29}$$

$$F_h(\phi_h) = l_{f,\Omega_i^*}(\phi_h) + \sum_{i=1}^{2} \frac{\eta\rho_i}{h} \int_{\partial\Omega_i^* \cap \partial\Omega} u_D \phi_h \, d\sigma. \tag{3.30}$$

Finally, our dG IgA scheme reads as follows: find $u_h^* \in V_h$ such that

$$A_h(u_h^*, \phi_h) = F_h(\phi_h), \quad \text{for all } \phi_h \in V_h. \tag{3.31}$$

Remark 7. Based on Remark 6, for the exact solution u it holds that

$$A_h(u, \phi_h) + R_{\Omega_{o21}}(u, \phi_h) - a_{res}(u, \phi_h) - F_h(\phi_h) = 0, \text{ for } \phi_h \in V_h. \tag{3.32}$$

Below, we quote a result that is useful for our later error analysis. For the proof we refer to [17], [19] and [18].

Lemma 1. *Under the assumption (2.21), there exist a positive constants C_1 and C_2 such that the estimates*

$$|R_{\Omega_{o21}}(u, \phi_h)| \le C_1 \|\phi_h\|_{dG} \, h^{\lambda - 0.5}, \quad |R_{\Omega_{o21}}(u^*, \phi_h)| \le C_2 \|\phi_h\|_{dG} \, h^{\lambda - 0.5}, \tag{3.33}$$

hold for the solutions u^* and u, and $\phi_h \in V_h$. The constants C_1 and C_2 do not depend on h.

Lemma 2. *The bilinear form $A_h(\cdot,\cdot)$ in (3.29) is bounded and elliptic on V_h, i.e., there are positive constants C_M and C_m such that the estimates*

$$A_h(v_h, \phi_h) \le C_M \|v_h\|_{dG} \|\phi_h\|_{dG} \quad \text{and} \quad A_h(v_h, v_h) \ge C_m \|v_h\|_{dG}^2, \tag{3.34}$$

hold for all v_h, $\phi_h \in V_h$ provided that η is sufficiently large.

Lemma 3. *Let $\beta = \lambda - \frac{1}{2}$. Then there is a constant $C = C(\eta, \rho) \ge 0$ independent of h such that the estimate*

$$A_h(w, \phi_h) \le C(\eta, \rho) \Big(\big(\|w\|_{dG}^2 + \sum_{i=1}^{N} h \, \rho_i \, \|\nabla w_i\|_{L^2(\partial\Omega_i^*)}^2 \big)^{\frac{1}{2}} + \mathcal{K}_o h^{\beta} \Big) \|\phi_h\|_{dG}, \tag{3.35a}$$

holds for all $w \in V_h^*$ and $\phi_h \in V_h$, where $\mathcal{K}_o = \|\nabla w\|_{L^2(\partial\Omega_{o21})} + \| \sum_{|\alpha|=2} |D^\alpha w| \|_{L^2(\Omega_{o21})}$.

In addition, if $v \in V$, see Assumption 1, then

$$A_h(v, \phi_h) \le C_1(\eta, \rho) \Big(\big(\|v\|_{dG}^2 + \sum_{i=1}^{2} h \, \rho_i \, \|\nabla v\|_{L^2(\partial\Omega_i^*)}^2 \big)^{\frac{1}{2}} + \mathcal{K}_{o,v} h^{\beta} \Big) \|\phi_h\|_{dG}, \tag{3.35b}$$

where $C_1(\eta, \rho)$ and $\mathcal{K}_{o,v}$ have similar form as in (3.35a).

Proof. The first estimate (3.35a) has been essentially proved in [17] and [19] for the case of having gap regions. For showing the second estimate, we can follow the same steps. We briefly mention the basic points. Since $v \in V$ the normal traces on the interfaces are well defined. Applying (2.1), we have

$$\Big|\sum_{i=1}^{2}\Big(\int_{\Omega_i^*}\rho_i\nabla v\cdot\nabla\phi_h\,dx\Big|\leq\Big(\sum_{i=1}^{2}\rho_i^{\frac{1}{2}}\|\nabla v\|_{L^2(\Omega_i^*)}\Big)\Big(\sum_{i=1}^{2}\rho_i^{\frac{1}{2}}\|\nabla\phi_h\|_{L^2(\Omega_i^*)}\Big). \tag{3.36}$$

Now, let us first show an estimate for the normal fluxes on F_{o21}. Using again (2.1), we obtain

$$\begin{aligned}&\Big|\sum_{F_{o21}}\int_{F_{o21}}\frac{1}{2}\big(\rho_2\nabla v+\rho_1\nabla v(\boldsymbol{\Phi}_{o21})\big)\cdot n_{F_{o21}}\phi_h\,d\sigma\Big|\\&\quad\leq c_\rho(\rho_2 h)^{\frac{1}{2}}\|\nabla v\|_{L^2(F_{o21})}\frac{\eta\{\rho\}}{h}\|\phi_h\|_{L^2(F_{o21})}+c_\rho c_{\boldsymbol{\Phi}_{o21}}(\rho_1 h)^{\frac{1}{2}}\|\nabla v\|_{L^2(F_{o12})}\frac{\eta\{\rho\}}{h}\|\phi_h\|_{L^2(F_{o21})}\\&\quad\leq C\Big(\sum_{i=1}^{2}h\,\rho_i\,\|\nabla v\|^2_{L^2(\partial\Omega_i^*)}\big)^{\frac{1}{2}}\Big)\|\phi_h\|_{dG}.\end{aligned} \tag{3.37}$$

Following the same steps as above, we can show

$$\begin{aligned}&\Big|\sum_{F_{o12}}\int_{F_{o12}}\frac{1}{2}\big(\rho_2\nabla v(\boldsymbol{\Phi}_{o12})+\rho_1\nabla v\big)\cdot n_{F_{o12}}\phi_h\,d\sigma\Big|\leq C_1\Big(\sum_{i=1}^{2}h\,\rho_i\,\|\nabla v\|^2_{L^2(\partial\Omega_i^*)}\big)^{\frac{1}{2}}\Big)\|\phi_h\|_{dG},\\&\Big|\sum_{i=1}^{2}\Big(\int_{\partial\Omega_i^*\cap\partial\Omega}\rho_i\nabla v\cdot n_{\partial\Omega_i^*}\phi_h\,d\sigma\Big|\leq C_2\Big(\sum_{i=1}^{2}h\,\rho_i\,\|\nabla v\|^2_{L^2(\partial\Omega_i^*)}\big)^{\frac{1}{2}}\Big)\|\phi_h\|_{dG},\\&\text{and}\qquad\Big|\sum_{i=1}^{2}\Big(\frac{\eta\{\rho\}}{h}\int_{F_{oij}}\big(v(\boldsymbol{\Phi}_{oij})-v\big)\phi_h\,d\sigma\Big)\Big|\leq C_3\sum_{F_{oij}\subset\partial\Omega_i^*}\frac{\{\rho\}}{h}\|v\|^2_{L^2(F_{oij})}\Big).\end{aligned} \tag{3.38}$$

Gathering together the above inequalities we can show (3.35b). ■

3.4 Discretization error analysis

Next, we discuss interpolation estimates that we will use to bound the discretization error. Let a function $v\in H^\ell(\mathcal{T}_H^*(\Omega_i))$ with $\ell\geq 2$. Under Assumptions 3, and using the results of [4] and [8], we can construct an interpolant $\Pi_h v$ such that the interpolation error semi-norm $|v-\Pi_h v|_{H^1(\Omega_i^*)}$, $i=1,2$, is well defined and the following estimate

$$\sum_{i=1,2}|v-\Pi_h v|_{H^1(\Omega_i^*)}\leq Ch^s\sum_{i=1,2}\|v\|_{H^\ell(\Omega_i^*)}, \tag{3.39}$$

holds, where $s=\min(\ell-1,p)$ and C depending on $p,\boldsymbol{\Phi}_i^*,\theta$ but not on h.

Lemma 4. *Let $v\in H^\ell(\mathcal{T}_H^*(\Omega_i))$ with $\ell\geq 2$ and let $\Pi_h v$ be the interpolation operator discussed above in (3.39). Then there exist constants $C_i>0$, $i=1,2$, depending on p, $\boldsymbol{\Phi}_i^*$, $i=1,2$ and the quasi-uniformity of the meshes but not on h such that*

$$\Big(\|v-\Pi_h v\|^2_{dG}+\sum_{i=1}^{2}h\|\nabla(v-\Pi_h v)\|^2_{L^2(\partial\Omega_i^*)}\Big)^{\frac{1}{2}}\leq\sum_{i=1}^{2}C_i h^s\|v\|_{H^\ell(\Omega_i^*)}, \tag{3.40}$$

where $s=\min(\ell-1,p)$.

Proof. The estimate (3.40) has been essentially proven in [17]. See also Lemma 10 in [25]. ■

Theorem 1. *Let $\beta = \lambda - \frac{1}{2}$ and $d_o = h^\lambda$ with $\lambda \geq 1$. Let $u^* \in H^\ell(\mathcal{T}_H^*(\Omega_i))$ with $\ell \geq 2$ be the solution of problem (3.2), and let $u_h^* \in V_h$ be the corresponding dG IgA solution of problem (3.31). Then the error estimate*

$$\|u^* - u_h^*\|_{dG} \lesssim h^r \big(\sum_{i=1}^{2} \|u\|_{H^\ell(\Omega_i^*)} \big), \tag{3.41}$$

holds, where $r = \min(s, \beta)$ with $s = \min(\ell - 1, p)$.

Proof. The proof is given in [17] and [19]. ■

Remark 8. The proceeding estimate is referred to the case where d_o is of order $\mathcal{O}(h^\lambda)$. If the width d_o is fixed, i.e., is not decreased as we refine the meshes, then, using (3.33), we can infer that the estimate (3.41) will take the form

$$\|u - u_h^*\|_{dG} \lesssim h^s + d_o\, h^{-\frac{1}{2}}, \tag{3.42}$$

where $s = \min(\ell - 1, p)$, see discussion in [17].

Main error estimate The estimate given in (3.41) concerns the distance between $u_h^* \in V_h$ and the solution $u^* \in H^\ell(\mathcal{T}_H^*(\Omega_i))$ with $\ell \geq 2$ of the perturbed problem (3.2) defined on $\mathcal{T}_H^*(\Omega)$. Based on (3.9) and (3.17), we show that a similar estimate holds for the physical solution u given by (2.8). Note that, by Assumption 1, we get that the solution u belongs to $(H^\ell(\Omega_{o21}) \cup H^\ell(\Omega_2)) \cap H^1(\Omega)$, with $\ell \geq 2$, i.e., $u \notin H^\ell(\Omega_2^*)$. Thus, first, we need to show an interpolation estimate similar to (3.39) for u. We utilize the interpolation estimates given in [9] and [8] for functions $u \in H^{\boldsymbol{\alpha}}_{\boldsymbol{\Phi}}(\Omega)$, see (2.24). For simplicity of our analysis, we present the results for the two-dimensional case, e.g., see Fig. 1(b),(c). Let us introduce the multi-indexes $\boldsymbol{\alpha} = (\alpha_1, \alpha_2) = (\ell, \ell)$ and $\boldsymbol{\gamma} = (\gamma_1, \gamma_2)$ with $|\boldsymbol{\gamma}| = 1$. Recalling Assumption 3 , Assumption 4 and Assumption 5, we can deduce that the solution $u \in H^{\boldsymbol{\alpha}}_{\boldsymbol{\Phi}_2^*}(\Omega_2^*)$ and $u \in H^{\boldsymbol{\alpha}}_{\boldsymbol{\Phi}_1^*}(\Omega_1^*)$, see Fig. 2. Finally, based on the interpolation estimates given in [9] and [8], e.g., see Section 4 in [8], we can construct an interpolant $\Pi_h u$, such that the estimates

$$|u - \Pi_h u|_{H^1(\Omega_2^*)} \leq C_2 \sum_{|\boldsymbol{\gamma}|=1} |u - \Pi_h u|_{\mathcal{H}^{\boldsymbol{\gamma}}_{\boldsymbol{\Phi}_2^*}(\Omega_2^*)} \leq C_2 h^s \|u\|_{\mathcal{H}^{\boldsymbol{\alpha}}_{\boldsymbol{\Phi}_2^*}(\Omega_2^*)}, \tag{3.43a}$$

$$|u - \Pi_h u|_{H^1(\Omega_1^*)} \leq C_1 \sum_{|\boldsymbol{\gamma}|=1} |u - \Pi_h u|_{\mathcal{H}^{\boldsymbol{\gamma}}_{\boldsymbol{\Phi}_1^*}(\Omega_1^*)} \leq C_1 h^s \|u\|_{\mathcal{H}^{\boldsymbol{\alpha}}_{\boldsymbol{\Phi}_1^*}(\Omega_1^*)}, \tag{3.43b}$$

holds, where $s = \min(\ell - 1, p)$ and C_1 and C_2 depending on $p, \boldsymbol{\Phi}_i^*, \theta$ but not on h. Having shown the interpolation estimates (3.43), then, we can follow the same steps as in [17], and [25], and to derive the interpolation estimate of interest

$$\begin{aligned} \|u - \Pi_h u\|^2_{dG,*} :=& \Big(\|u - \Pi_h u\|^2_{dG} + \sum_{i=1}^{2} h\rho_i \, \|\nabla(u - \Pi_h u)\|^2_{L^2(\partial\Omega_i^*)} \Big)^{\frac{1}{2}} \\ &\leq \sum_{i=1}^{2} C_i h^s \|u\|_{\mathcal{H}^{\boldsymbol{\alpha}}_{\boldsymbol{\Phi}_i^*}(\Omega_i^*)}, \end{aligned} \tag{3.44}$$

where $s = \min(\ell - 1, p)$ and C_i depending on $p, \boldsymbol{\Phi}_i^*, \theta$, but not on h.

Theorem 2 (main error estimate). *Let the multi-index* $\boldsymbol{\alpha} = (\alpha_1, \alpha_2) = (\ell, \ell)$ *as above. The following error estimate holds*

$$\|u - u_h^*\|_{dG} \leq C\Big(h^s \sum_{i=1}^{2} \|u\|_{\mathcal{H}^{\boldsymbol{\alpha}}_{\boldsymbol{\Phi}_i^*}(\Omega_i^*)} + d_o \|f\|_{L^2(\Omega_{o21})} + h^\beta \mathcal{K}_o\Big), \tag{3.45}$$

where $\beta = \lambda - \dfrac{1}{2}$, $s = \min(\ell - 1, p)$, *and* C *depends on the constants in (3.44), (3.35a) and (3.34).*

Proof. Let $z_h \in V_h$ and let u be the exact solution. By the definition of the discrete dG IgA scheme in (3.31) and (3.32), we have

$$\begin{aligned} A_h(u_h^* - z_h, \phi_h) &= A_h(u, \phi_h) + R_{\Omega_{o21}}(u, \phi_h) - a_{res}(u, \phi_h) - F_h(\phi_h) - A_h(z_h, \phi_h) + F_h(\phi_h) \\ &= A_h(u - z_h, \phi_h) + R_{\Omega_{o21}}(u, \phi_h) - a_{res}(u, \phi_h). \end{aligned} \tag{3.46}$$

Setting above $\phi_h = u_h^* - z_h$, using the coercivity and boundedness of $A_h(\cdot, \cdot)$ described in (3.34) and (3.35b), and using also the bounds in (3.17) and (3.33), we can finally obtain

$$c_e \|u_h^* - z_h\|_{dG}^2 \leq c_b \|u - z_h\|_{dG,*} \|u_h^* - z_h\|_{dG} + c_2 d_o \|f\|_{L^2(\Omega_{o21})} \|u_h^* - z_h\|_{dG} + c_3 h^{\lambda - \frac{1}{2}} \|u_h^* - z_h\|_{dG}. \tag{3.47}$$

Setting in (3.47), $z_h = \Pi_h u$, using estimate (3.44), and applying triangle inequality

$$\|u - u_h^*\|_{dG} \leq \|u - \Pi_h u\|_{dG,*} + \|\Pi_h u - u_h^*\|_{dG}, \tag{3.48}$$

the desired estimate follows.

■

4 Numerical tests

In this section, we perform several numerical tests with different shapes of overlapping regions as well as combinations with inhomogeneous diffusion coefficients for two- and three- dimensional problems. We investigate the order of accuracy of the dG IgA scheme proposed in (3.29). All examples have been performed using second degree ($p = 2$) B-spline spaces. We present the asymptotic behaviour of the error convergence rates for widths $d_o = h^\lambda$ with $\lambda \in \{1, 2, 2.5, 3\}$. Every example has been solved applying several mesh refinement steps with $\ldots, h_i, h_{i+1}, \ldots$, satisfying Assumption 2. The numerical convergence rates r have been computed by the ratio $r = \frac{\ln(e_i/e_{i+1})}{\ln(h_i/h_{i+1})}$, $i = 1, 2, \ldots$, where the error $e_i := \|u - u_h^*\|_{dG}$ is always computed on the meshes $\cup_{i=1}^2 T^{(i)}_{h_i, \Omega_i^*}$. We mention that, in the test cases, we use highly smooth solutions on each patch, i.e., $p + 1 \leq \ell$, and therefore the order s in (3.41) and (3.45) becomes $s = p$. The predicted values of power β, the order s and the expected convergence rate r, for several values of λ, are displayed in Table 1. In any test case, the overlap regions are artificially created by moving the control points, which are related to the interfaces F_{ij}, in the direction of $n_{F_{ij}}$ or of $-n_{F_{ij}}$.

All tests have been performed in G+SMO [26], which is a generic object-oriented C++ library for IgA computations, [23, 24]. In Section 3, we developed and provided a rigorous analysis for the dG IgA method (3.31) which includes a non-symmetric numerical flux. In the materialization of the method, we utilized the associated symmetrised version the numerical flux, [32]. For solving the resulting linear system, we use the dG-IETI-DP method presented in [16], see also [14] for an analysis of the method and [15] for results on parallel scalability.

Although in the analysis, we consider meshes with similar quasi-uniform patch-wise properties, it is known that the introduction of dG techniques on the subdomain interfaces makes the

use of non-matching and non-uniform meshes easier, see [25]. Keeping a constant linear relation between the sizes of the different patch meshes, the approximation properties of the method are not affected, see [25]. In the examples below, we exploit this advantage of the dG methods and first solve two-dimensional problems considering non-matching meshes. The convergence rates are expected to be the same as those displayed in Table 1.

	B-spline degree p			
	Smooth solutions, $u \in H^{\ell \geq p+1}$			
$d_o = h^\lambda$	$\lambda = 1$	$\lambda = 2$	$\lambda = 2.5$	$\lambda = 3$
$\beta :=$	0.5	1.5	2	2.5
$s :=$	p	p	p	p
$r :=$	0.5	1.5	$\min(p, \beta)$	$\min(p, \beta)$

Table 1. The values of the expected rates r as they result from estimate (3.45).

4.1 Two-dimensional numerical examples

The control points with the corresponding knot vectors of the domains given in Example 1-3 are available under the names `yeti_mp2`, `12pSquare` and `bumper` as `.xml` files in G+SMO[1].

Example 1: uniform diffusion coefficient $\rho_i = 1$, $i = 1, \ldots, N$. The first numerical example is a simple test case demonstrating the applicability of the proposed technique for constructing the dG IgA scheme on segmentations including overlaps with general shape. The domain Ω with the $N = 21$ subdomains Ω_i^* and the initial mesh are shown in Fig. 3(a). We note that we consider non-matching meshes across the interior interfaces. The Dirichlet boundary condition and the right hand side f are determined by the exact solution $u(x, y) = \sin(\pi(x + 0.4)/6)\sin(\pi(y + 0.3)/3) + x + y$. In this example, we consider the homogeneous diffusion case, i.e., $\rho_i = 1$ for all Ω_i^*, $i = 1, \ldots, N$.

We performed four groups of computations, where for every group the maximum size of d_o was defined to be $\mathcal{O}(h^\lambda)$, with $\lambda \in \{1, 2, 2.5, 3\}$. In Fig. 3(b) we present the discrete solution for $d_0 = h$. Since we are using second-order ($p = 2$) B-spline space, based on Table 1, we expect optimal convergence rates for $\lambda = 2.5$ and $\lambda = 3$. The numerical convergence rates for several levels of mesh refinement are plotted in Fig. 3(c). They are in very good agreement with the theoretically predicted estimates given in Theorem 2, see also Table 1. We observe that we have optimal rates r for the cases where $\lambda \geq 2.5$ and sub-optimal for the rest values of λ.

Example 2: different diffusion coefficients $\rho_1 \neq \rho_2$. In the second example, we consider a rectangular domain Ω, that is described as a union of $N = 12$ patches, see Fig. 4(a). Here, we study the case of having smooth solutions on each Ω_i but discontinuous coefficient, i.e., we set $\rho_i = 3\pi/2$ for the patches belonging to half plane $x \leq 0$ and we set $\rho_i = 2$ for the rest patches according to the pattern in Fig. 4(a). By this example, we numerically validate the predicted convergence rates on $\mathcal{T}_H^*$ with overlaps, for the case of having smooth solutions and discontinuous coefficient ρ. The exact solution is given by the formula

$$u(x, y) = \begin{cases} \sin(\pi(2x + y)) & \text{if } x < 0 \\ \sin(\pi(\frac{3\pi}{2}x + y)) & \text{otherwise.} \end{cases} \tag{4.1}$$

The boundary conditions and the source function f are determined by (4.1). Note that in this test case, we have $[\![u]\!]|_{F_{ij}} = 0$ as well $[\![\rho \nabla u]\!]|_{F_{ij}} \cdot n_{F_{ij}} = 0$ for all the interior interfaces F_{ij}.

[1] G+SMO: https://www.gs.jku.at/trac/gismo

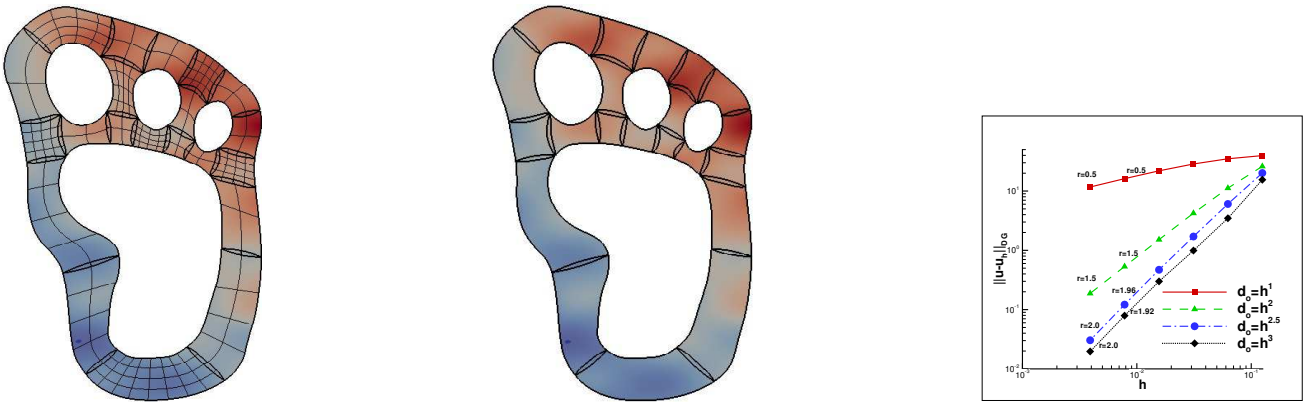

(a) (b) (c)

Fig. 3. Example 1: (a) The patches Ω_i^* with the initial non-matching meshes and the contours of the exact solution. (b) The contours of the u_h^* solution for $d_o = h$. (c) The convergence rates for the different values of λ.

The problem has been solved on a sequence of meshes with $h_0, ..., h_i, h_{i+1}, ...$, following a sequential refinement process, i.e., $h_{i+1} = \dfrac{h_i}{2}$, where we set $d_o = h_i^\lambda$, with $\lambda \in \{1, 2, 2.5, 3\}$. For the numerical tests, we use B-splines of the degree $p = 2$. Hence, we expect optimal rates for $\lambda \geq 2.5$. In Fig. 4(b) the approximate solution u_h^* is presented on a relative coarse mesh with $d_o = 0.06$. The results of the computed rates are presented in Fig. 4(c). For all test cases, we can observe that our theoretical results presented in Table 1 are confirmed.

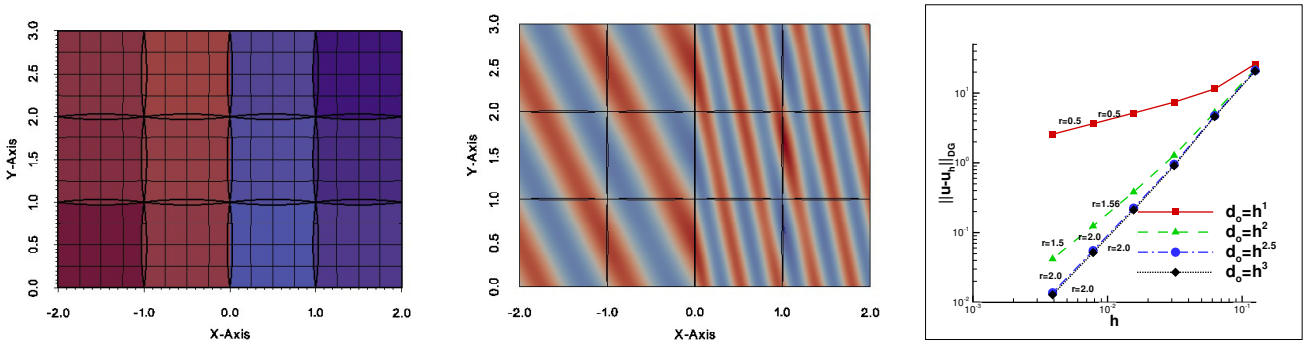

(a) (b) (c)

Fig. 4. Example 2: (a) The overlapping patches Ω_i^* and the pattern of diffusion coefficients ρ_i, (b) The contours of u_h^* on every Ω_i computed with $d_0 = 0.06$, (c) The convergence rates for the 4 choices of λ.

4.2 Three-dimensional numerical examples

As a final example, we consider a three-dimensional test. The domain Ω has been constructed by a straight prolongation to the z-direction of a two dimensional (curved) domain, see Fig. 5(a). The two physical domains Ω_1 and Ω_2 have the physical interface F_{12} consisting of all points (x, y, z) such that $-1 \leq x \leq 0$, $x + y = 0$ and $0 \leq z \leq 1$, see Fig. 5(a). The knot vector in z-direction is simply $\Xi_i^3 = \{0, 0, 0, 0.5, 1, 1, 1\}$ with $i = 1, 2$. We solve the problem using matching meshes, as depicted in Fig. 5(a). The B-spline parametrizations of these domains are constructed by adding a third component to the control points with the following values $\{0, 0.5, 1\}$. The completed knot vectors $\boldsymbol{\Xi}_{i=1,2}^{k=1,2,3}$ together with the associated control nets can be found in G+SMO library in the file `bumper.xml`. The overlap region is artificially constructed by moving only the interior control points located at the interface into the normal direction $n_{F_{12}}$ of the related interface F_{12}. Due to the fact that the overlap has to be inside of the domain, we have to provide cuts though

the domain in order to visualize them, cf. Fig. 5(b). The Dirichlet boundary conditions u_D and the right hand side f, see (2.3), are chosen such that the exact solution is

$$u(x,y,z) = \begin{cases} \sin(\frac{\pi}{2}(x+y)) & \text{if } (x,y) \in \Omega_1, \\ e^{\sin(x+y)} & \text{if } (x,y) \in \Omega_2. \end{cases} \tag{4.2}$$

with diffusion coefficient $\rho = \{1, \pi/2\}$. Note that the interfaces conditions (2.7) are satisfied. The two physical subdomains, the initial matching meshes and the exact solution are illustrated in Fig. 5(a). We construct an overlap region with $d_o = 0.5$ and solve the problem using $p = 2$ B-spline functions. In Fig. 5(b), we show the domain meshes $T^{(i)}_{h_i,\Omega_i^*}$, $i = 1, 2$, the overlapped meshes in Ω_{o12} and we plot the contours of the produced solution u_h^* for the interior plane $z = 0.5$. We can see that, both faces of $\partial\Omega_{o12}$ are not parallel to the Cartesian axes. Moreover, we point out that the problem has been solved using non matching meshes on the overlapping interfaces. We have computed the convergence rates for four different values $\lambda \in \{1, 2, 2.5, 3\}$ related to the overlapping region width $d_o = h^\lambda$. The results of the computed rates are plotted in Fig. 5(c). We observe from the plots that the rates r are in agreement with the rates predicted by the theory, see estimate (3.45) and Table 1.

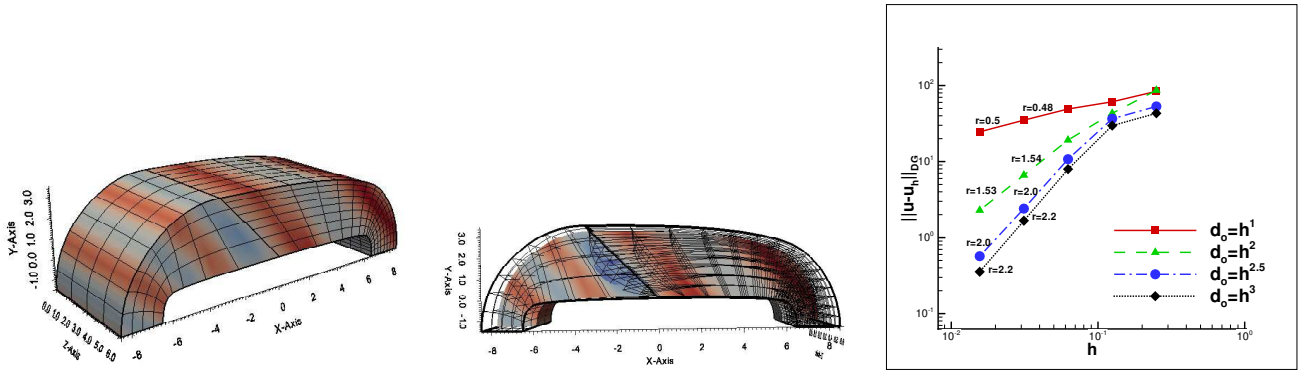

(a) (b) (c)

Fig. 5. Example 4, $\Omega \subset \mathbb{R}^3$: (a) The physical patches with an initial coarse mesh and the contours of the exact solution, (b) The contours of u_h^* computed on $\Omega_1^* \cup \Omega_2^*$ with $d_o = 1.5$, (c) Convergence rates r for the four values of λ.

5 Conclusions

In this article, we have proposed and analyzed a dG IgA scheme for discretizing linear, second-order, diffusion problems on IgA patch decompositions with non-matching interface parametrizations, which result to the appearance of overlapping regions. This type of decompositions lead to the use of different diffusion coefficients on the overlapping patches. Auxiliary problems were introduced in every patch and dG IgA methodology applied for discretizing these problems. The normal fluxes on the overlapped interior faces were appropriately modified using Taylor expansions, and these fluxes were further used to construct numerical fluxes in order to couple the associated discrete dG IgA problems. The method were successfully applied to the discretization of the diffusion problem in cases with complex overlaps using non-matching grids. A priori error estimates in the dG-norm were shown in terms of the mesh-size h and the maximum width d_o of the overlapping regions. The estimates were confirmed by solving several two- and three-dimensional test problems with known exact solutions.

Acknowledgments

The authors wish to thank Prof. Ulrich Langer and Prof. Dirk Pauly for many interesting discussions. This work was supported by the Austrian Science Fund (FWF) under the grant NFN S117-03 and W1214-N15, project DK4.

References

1. A. Hansbo, P. Hansbo, and M. G. Larson. A finite element method on composite grids based on Nitsche's method. *ESAIM: M2AN*, 37(3):495–514, 2003.
2. A.Massing, M. G. Larson, and A. Logg. Efficient Implementation of Finite Element Methods on Nonmatching and Overlapping Meshes in Three Dimensions. *SIAM J. Sci. Comput., (Software and High-Performance Computing)*, 35(1):C23–C47655 – 660, 2013.
3. A. Apostolatos, R Schmidt, R. Wüchner, and K. U. Bletzinger. A Nitsche-type formulation and comparison of the most common domain decomposition methods in isogeometric analysis. *Int. J. Numer. Meth. Engng*, 97:473–504, 2014.
4. Y. Bazilevs, L. da Veiga Beirão, J. A. Cottrell, T.J.R. Hughes, and G. Sangalli. Isogeometric analysis: approximation, stability and error estimates for h-refined meshes. *Math. Mod. Meth. Appl. Sci.*, 16(7):1031–1090, 2006.
5. Y. Bazilevs and T.J.R. Hughes. Weak imposition of dirichlet boundary conditions in fluid mechanics. *Computers and Fluids*, 36(1):12 – 26, 2007.
6. F. Brezzi, J.-L. Lions, and O. Pironneau. Analysis of a Chimera method. *Comptes Rendus de l'Académie des Sciences - Series I - Mathematics*, 332(7):655 – 660, 2001.
7. J. A. Cotrell, T.J.R. Hughes, and Y. Bazilevs. *Isogeometric Analysis, Toward Integration of CAD and FEA*. John Wiley and Sons, Sussex, United Kingdom, 2009.
8. L. da Veiga Beirão, A. Buffa, G. Sangalli, and R. Vázquez. Mathematical analysis of variational isogeometric methods. *Acta Numerica*, 23:157–287, 5 2014.
9. L. da Veiga Beirão, D. Cho, and G. Sangalli. Anisotropic NURBS approximation in isogeometric analysis. *Comput. Methods Appl. Mech. Engrg.*, 209–212:1–11, 2012.
10. C. De-Boor. *A Practical Guide to Splines*, volume 27 of *Applied Math. Science*. Springer, New York, 2 edition, 2001.
11. M. Dryja. On discontinuous Galerkin methods for elliptic problems with discontinuous coefficients. *Comput. Meth. Appl. Math.*, 3(1):76–85, 2003.
12. A. Ern and J.-L. Guermond. *Theory and Practice of Finite Elements*, volume 159 of *Applied Mathematical Sciences*. Springer-Verlag New York, 2004.
13. L. C. Evans. *Partial Differential Equestions*, volume 19 of *Graduate Studies in Mathematics*. American Mathematical Society, 1st Edition edition, 1998.
14. C. Hofer. Analysis of discontinuous Galerkin dual-primal isogeometric tearing and interconnecting methods. Technical Report No. 2016-03, https://www.dk-compmath.jku.at/publications/dk-reports/2016-11-03, DK Computational Mathematics Linz Report Series, 2016.
15. C. Hofer. Parallelization of continuous and discontinuous Galerkin dual-primal isogeometric tearing and interconnecting methods. Technical Report No. 2016-02 https://www.dk-compmath.jku.at/publications/dk-reports/2016-11-02, DK Computational Mathematics Linz Report Series, 2016.
16. C. Hofer and U. Langer. Dual-primal isogeometric tearing and interconnecting solvers for multipatch dG-IgA equations. *Computer Methods in Applied Mechanics and Engineering*, 316":2 – 21, 2017.
17. C. Hofer, U. Langer, and I. Toulopoulos. Discontinuous Galerkin isogeometric analysis of elliptic diffusion problems on segmentations with gaps. *SIAM J. SCI. COMPUT.*, 38:A3430 – A3460, 2016.
18. C. Hofer, U. Langer, and I. Toulopoulos. Discontinuous Galerkin isogeometric analysis on non-matching segmentation: Error estimates and efficient solvers. RICAM report No. 2016-23, http://www.ricam.oeaw.ac.at/publications/ricam-reports/, 2016.
19. C. Hofer and I. Toulopoulos. Discontinuous Galerkin Isogeometric Analysis of Elliptic Problems on Segmentations with Non-matching Interfaces. *Computers and Mathematics with Applications*, 72(7):1811–1827, 2016.
20. J. Hoschek and D. Lasser. *Fundamentals of Computet Aided Geometric Design*. A K Peters, Wellesley, Massachusetts, 1993. Translated by L. Schumaker.
21. T.J.R. Hughes, J. A. Cottrell, and Y. Bazilevs. Isogeometric analysis : CAD, finite elements, NURBS, exact geometry and mesh refinement. *Comput. Methods Appl. Mech. Engrg.*, 194:4135–4195, 2005.
22. B. Jüttler, M. Kapl, D.-M. Nguyen, Q. Pan, and M. Pauley. Isogeometric segmentation: The case of contractible solids without non-convex edges. *Computer-Aided Design*, 57:74–90, 2014.
23. B. Jüttler, U. Langer, A. Mantzaflaris, S.E. Moore, and W. Zulehner. Geometry + Simulation Modules: Implementing Isogeometric Analysis. *PAMM*, 14(1):961–962, 2014.
24. U. Langer, A. Mantzaflaris, St. E. Moore, and I. Toulopoulos. *Multipatch Discontinuous Galerkin Isogeometric Analysis*, volume 107 of *Lecture Notes in Computational Science and Engineering*, pages 1–32. Springer International Publishing, Heidelberg, 2015.
25. U. Langer and I. Toulopoulos. Analysis of Multipatch Discontinuous Galerkin IgA Approximations to Elliptic Boundary Value Problems. *Computing and Visualization in Science*, 17(5):217–233, 2016.
26. A. Mantzaflaris, C. Hofer, et al. G+SMO (Geometry plus Simulation MOdules) v0.8.1. http://gs.jku.at/gismo, 2015.

27. T. Mathew. *Domain Decomposition Methods for the Numerical Solution of Partial Differential Equations (Lecture Notes in Computational Science and Engineering)*, volume 61. Springer Publishing Company, 1 edition, 2008.
28. V. P. Nguyen, P. Kerfriden, M. Brino, S. P. A. Bordas, and E. Bonisoli. Nitsche's method for two and three dimensional NURBS patch coupling. *Computational Mechanics*, 53(6):1163–1182, 2014.
29. M. Pauley, D.-M. Nguyen, D. Mayer, J. Speh, O. Weeger, and B. Jüttler. The isogeometric segmentation pipeline. In B. Jüttler and B. Simeon, editors, *Isogeometric Analysis and Applications IGAA 2014*, volume 107 of *Lecture Notes in Computer Science*, Heidelberg, 2015. Springer.
30. C. Pechstein. *Finite and boundary element tearing and interconnecting solvers for multiscale problems.* Berlin: Springer, 2013.
31. D. A. Di Pietro and A. Ern. *Mathematical Aspects of Discontinuous Galerkin Methods (Mathmatiques et Applications)*, volume 69 of *Mathmatiques et Applications*. Springer-Verlag, 2010.
32. B. Riviere. *Discontinuous Galerkin methods for Solving Elliptic and Parabolic Equations*. SIAM, Society for industrial and Applied Mathematics Philadelphia, 2008.
33. M. Ruess, D. Schillinger, A. I. Özcan, and E. Rank. Weak coupling for isogeometric analysis of non-matching and trimmed multi-patch geometries. *Computer Methods in Applied Mechanics and Engineering*, 269(0):46 – 71, 2014.
34. L. L. Schumaker. *Spline Functions: Basic Theory*. Cambridge, University Press, third Edition edition, 2007.
35. A. Tagliabue, L. Dedé, and A. Quarteroni. Isogeometric analysis and error estimates for high order partial differential equations in fluid dynamics. *Computers and Fluids*, 102:277 –303, 2014.